Available online at www.sciencedirect.com
SCIENCE DIRECT
Journal of Asian Earth Sciences 28 (2006) 439–456
Journal of Asian Earth Sciences
www.elsevier.com/locate/jaes

Juxtaposition of adakite, boninite, high-TiO_2 and low-TiO_2 basalts in the Devonian southern Altay, Xinjiang, NW China

Hecai Niu [a], Hiroaki Sato [b,*], Haixiang Zhang [a,*], Jun'ichi Ito [b], Xueyuan Yu [a], Takashi Nagao [c], Kentaro Terada [d], Qi Zhang [e]

[a] *Guangzhou Institute of Geochemistry, Chinese Academy of Science, 510640 Guangzhou, People's Republic of China*
[b] *Department of Earth and Planetary Sciences, Graduate School of Science and Technology, Kobe University, Rokko-dai 1-1, Nada, Kobe 657-8501, Japan*
[c] *Department of earth sciences, Faculty of science, Yamaguchi University, Yoshida 1677-1, Yamaguchi 753-8526, Japan*
[d] *Graduate School of Science, Hiroshima University, Higashi-Hiroshima 739-8526, Japan*
[e] *Institute of Geology and Geophysics, Chinese Academy of Science, P.O. Box 9825, Beijing 100029, People's Republic of China*

Received 30 December 2004; received in revised form 3 October 2005; accepted 14 November 2005

Abstract

We present petrographic and geochemical data on representative samples of the Devonian adakite, boninite, low-TiO_2 and high-TiO_2 basalts and associated rocks in the southern Altay areas, Xinjiang, NW China. These volcanic rocks mostly occur as tectonic blocks within suture zones between the Siberian and Junggar plates. Adakite occurs in the Suoerkuduke area ca. 40 km south of Fuyun, and actually represents a poorly-sorted massive volcaniclastic deposit, mostly consisting of a suite of hornblende andesite to pyroxene andesite. The geochemical features of the adakite suggest its generation by melting of subducted oceanic crust. Boninite occurs in the Saerbulake area ca. 20 km southwest of Fuyun, as pillowed lava or pillowed breccia. It is associated with high-TiO_2 basalt/gabbro and low-TiO_2 basalt. The boninites are metamorphosed, but contain relict clinopyroxene with Mg# (=100*Mg/(Mg+Fe)) of 90–92, and Cr_2O_3 contents of 0.5–0.7 wt% and chromian spinel with Cr/(Cr+Al) ratio of 0.84. The bulk rock compositions of the boninites are characterized by low and U-shaped REE with variable La/Yb ratios. They are classified as high-Ca boninite. The Cr-rich cpx phenocryst and Chromian spinel suggests that the boninites were formed by melting of mildly refractory mantle peridotite fluxed by a slab-derived fluid component under normal mantle potential temperature conditions. Basaltic rocks occur as massive flows, pillowed lavas, tuff breccia, lapilli tuff and blocks in tectonic mélanges. Together with gabbros, the basaltic rocks are classified into high-TiO_2 (>1.7 wt%) and low-TiO_2 (<1.5 wt%) types. They show variable trace element compositions, from MORB-type through transitional back-arc basin basalt to arc tholeiite, or within plate alkalic basalt. A notable feature of the Devonian formations in the southern Altay is the juxtaposition of volcanic rocks of various origins even within a limited area; i.e. the adakite and the boninites are associated with high-TiO_2 and low-TiO_2 basalts and/or gabbros, respectively. This is most likely produced by complex accretion and tectonic processes during the convergence in the Devonian–Carboniferous paleo-Asian Ocean between the Siberian and Junggar plates.

Keywords: Altay; Boninite; Adakite; Basalts; Devonian

1. Introduction

Şengör et al. (1993) proposed that the Altaid between the Sino-Korean and Siberian cratons occupies a unique position in the formation of new crustal blocks. In the Altaid or the Central Asian Orogenic Belt (CAOB), both lateral accretion of arc complexes and vertical accretion of underplated material of mantle derivation rapidly produced juvenile continental crust during the Paleozoic (Jahn et al., 2004). Jahn et al. (2000) pointed out that the juvenile nature of granitic rocks of the CAOB, based on the Nd–Sr isotopic signatures, reinforces the massive creation of new continental crust in the area. Although there are several microcratons or oceanic crustal fragments occurring between the Sino-Korean and Siberian cratons, such as the Junggar and Mongolian microplates (Zonenshain and Savostin, 1981; Chen and Jahn, 2004), the wide distribution of Paleozoic formations in the Altaid area points to the need for further geological, chronological, petrological and geophysical

* Corresponding authors.
E-mail addresses: hsato@kobe-u.ac.jp (H. Sato), zhanghx@gig.ac.cn (H. Zhang).

1367-9120/$ - see front matter © 2006 Elsevier Ltd. All rights reserved.
doi:10.1016/j.jseaes.2005.11.010

investigations in order to understand the mode of crustal formation and termination in the Altaids. In the present work, we present new geochemical and petrological data on the Devonian volcanic and plutonic rocks along the southern margin of the Altay Mountains. We identified boninite, adakite, high-TiO_2 and low-TiO_2 basalts and gabbros, peridotite, and granitic rocks in the area. Similar volcanic rock associations have been found in the neighborhood of the Altay area, including Paleozoic ophiolites in the Kunlun Mountains (Yang et al., 1996; Wang et al., 2001), and the eastern Sayan range of Mongolia/Russia (Robinson et al., 1999; Zhou et al., 2001). Adakites were found in the Qinling Mountains (Zhang et al., 1998) and in Tianshan (Xiong et al., 2001). Hu et al. (2000) examined the Phanerozoic crustal evolution of northern Xinjiang through geochemical data and Nd isotopes of granitic rocks. These studies showed arc-related igneous activity along the Mongolia, Altay to Kunlun Mountains throughout the Paleozoic. Some MORBs or back-arc basin basalts were identified in the volcanic sequences. Niu et al. (1999) reported boninitic dacites in the Ashle area of southern Altay. These rocks are characterized by low and U-shaped REE patterns, suggesting magma generation from a strongly depleted source. We already described the geochemistry of adakite and Nb-enriched basalt and their tectonic implications (Zhang et al., 2005). The purpose of this work is to further describe new occurrences of boninites, and varieties of basalts, gabbros, and a peridotite, together with some geological and petrographic features of the adakite. We discuss the conditions of generation of these volcanic and plutonic rocks, and their tectonic significances.

2. Geological occurrences

Our field study was conducted in five areas along the southern margin of the Altay Mountains of Xinjiang, China. They are named from southeast to northwest; Suoerkuduke, Saerbulake, Kuerti, Kekesentao, and Ashele areas as shown in Fig. 1. The geological occurrence and rock association are described as follows.

2.1. Suoerkuduke

In the Suoerkuduke area (Fig. 1), adakitic rocks are found in association with basalt, andesite, diorite, dolerite and limestone. These rocks occur in spotted areas of 10×10 km without any obvious stratigraphic relationship. We interpret them as components of a tectonic mélange or an olistostrome deposit. The adakitic rocks occur in an outcrop of 20×30 m, comprising the top of a low mound ca. 10 m high (46°31,55′N, 89°34.64′E). They are dark gray, massive and compact rocks, and are actually massive tuffaceous clastic deposits with thicknesses of more than 5 m. They consist of sporadic lapilli-size lithic fragments of

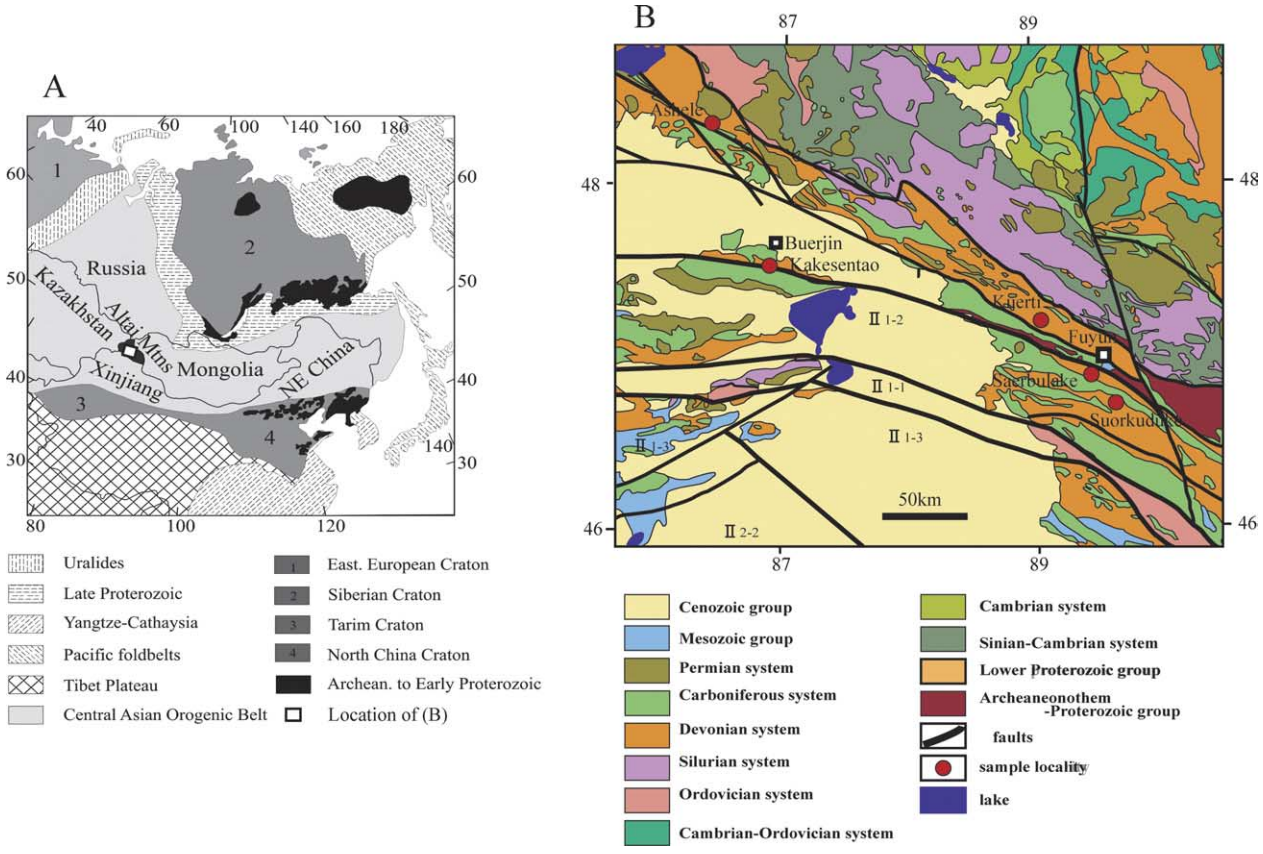

Fig. 1. (A) Distribution of Altaid belt in central Asia after Şengör et al. (1993) and (B) Geological map (after Wang et al., 1995) and locality of the samples used in the present work in the southern Altay Mountains, Xinjiang, northwestern China.

pyroxene andesite and hornblende andesite, set in dark fine-grained matrix. The fragments are generally angular to subangular, and are poorly sorted, suggesting temporal and massive deposition. Adjacent to the adakitic rocks, altered basalt to andesite, and microdiorite to dolerite occur in close association. Some of them represent volcanoclastic deposits, and others massive lavas or hypabyssal rocks. Limestone occurs in one outcrop of ca. 30 m across, in which fossils of Crinoids of Devonian age are ubiquitously found. Sedimentary rocks are scarce in the Devonian formation of the Suoerkuduke area.

2.2. Saerbulake

We investigated 10 outcrops within an area of 15 km east–west and 8 km north–south in the Saerbulake area (Fig. 1). Four outcrops consist of sedimentary rocks of sandstone and shale. Other outcrops are composed mostly of igneous rocks. These consist of rock fragments of basalt, andesite, boninite, volcanic tuff, and dolerite-gabbro, and may represent a mélange deposit. Each or some rock types represent a small outcrop, but neighboring outcrops, several tens of meters apart, show different rock types near the top of mounds. The rocks are massive, compact, and dark-colored, but some show epiclastic texture. The epiclastic rocks consist of angular fragments of crystals and rocks, and are poorly sorted. Two kinds of boninitic rocks were identified in Saerbulake; one is massive lava occurring together with basaltic tuff and gabbros, and the other is pillowed lava or pillowed breccias of boninitic composition. Pillowed lavas and breccias are identified by the presence of chilled margins and radial cracks.

2.3. Kuerti

Xu et al. (2003) reported petrological and geochemical studies of Kuerti meta-igneous rocks, and ascribed their generation in a back-arc basin environment. We surveyed a 10 km section along the Kuerti river to the southwest of Kuerti (Fig. 1). The section is divided into a northeast sequence and southwest layered sequence, separated by migmatitic gneiss. The migmatitic gneiss is a massive, medium grained rock often with mylonitic shear textures. The overlying northeast sequence consists of pillowed lavas and hyaloclastite, volcanic sediments, radioralian chert, which were metamorphosed to greenschist facies. The southwest sequence is mainly composed of alternating layers of leucocratic gneissose granite several centimeter to 2 m thick and melanocratic greenschist to amphibolite. The boundary between the granite and amphibolite is sharp, and may represent sheeted dikes of granitic magma intruded into the mafic rocks.

2.4. Kekesentao

The Kekesentao area (Fig. 1) shows a hummocky topography. The rocks in the Kekesentao area are similar to those of Suoerkuduke and Saerbulake; i.e. rocks occur as mélange or oliststrome deposits. Rock types in the area include peridotite, amphibolite, diorite, cataclastic granite, hornfels, coarse sandstone, limestone and dacitic welded tuff. The peridotite occurs together with limestone, and sedimentary rocks (mainly sandstone) occur in neighboring outcrops.

2.5. Ashele

Niu et al. (1999) found boninitic dacite and basalt in a deep core of the Ashele mine. The present field investigation was carried out on the surface outcrops of the Ashele area, spanning 86°32.7′–86°36.1′ East, and 48°28.2′–48° 32.3′ North for a total area of 3×3 km^2. Most of the outcrops are massive, but some epiclastic deposits show variable strike and dip, and strong deformation with north–south fold axes. The rocks in the Ashele surface outcrops consist of basaltic pillow lava, hyaloclastite, microdiorite, quartz porphyry, massive lavas to lapilli tuff of basalt, and massive dacite lava.

3. Petrography and mineralogy

3.1. Adakite

Although adakite was defined on the basis of bulk rock chemical compositions (Defant and Drummond, 1990), it has petrographic characteristics common to calc-alkalic intermediate to silicic rocks. In the present study, we identified adakitic rocks in an outcrop in the Suoerkuduke area (#0601; notation of sample number corresponds to that in Table 2). It actually represents a massive, fine-grained volcaniclastic rock, consisting predominantly of lithic fragments of hornblende andesite and pyroxene andesite, with subordinate mineral grains of plagioclase, hornblende, augite, quartz, magnetite, and rare calcareous microfossils (Fig. 2A). Most of the fragments are angular to subangular, and are poorly sorted. Although the adakitic volcaniclastic rock is classified as a heterolithic clastic deposit, most of the constituent fragments (>99%) are derived from a suite of adakitic lavas. Representative analyses of hornblende are presented in Table 1. Plagioclase constitutes about 20 vol% of the rock, and is altered to albite-oligoclase (Ca/(Ca+Na)=0.02–0.25). Hornblende is fresh and its modal content is ca. 5 vol%. It can be classified as magnesio-hornblende. Phenocryst clinopyroxene is fresh and idiomorphic, and constitutes ca. 3–5 vol% of the rock. The groundmass is hyalopilitic with tachylytic glass to fine-grained holocrystallline textures.

3.2. Boninite

Boninite is a high-magnesian andesite depleted in high field strength elements and somewhat enriched in large-ion-lithophile elements relative to mid-oceanic ridge basalts (Crawford et al., 1989). Petrographically, fresh boninite of the Bonin Island contain phenocrysts of olivine, clinoenstatite (inverted from protoenstatite), orthopyroxene, and augite, while the groundmass consists of orthopyroxene, augite, pigeonite and glass (Shiraki et al., 1980). The boninitic rocks of the Saerbulake area (46°55.22′N, 89°16.03′E), southern

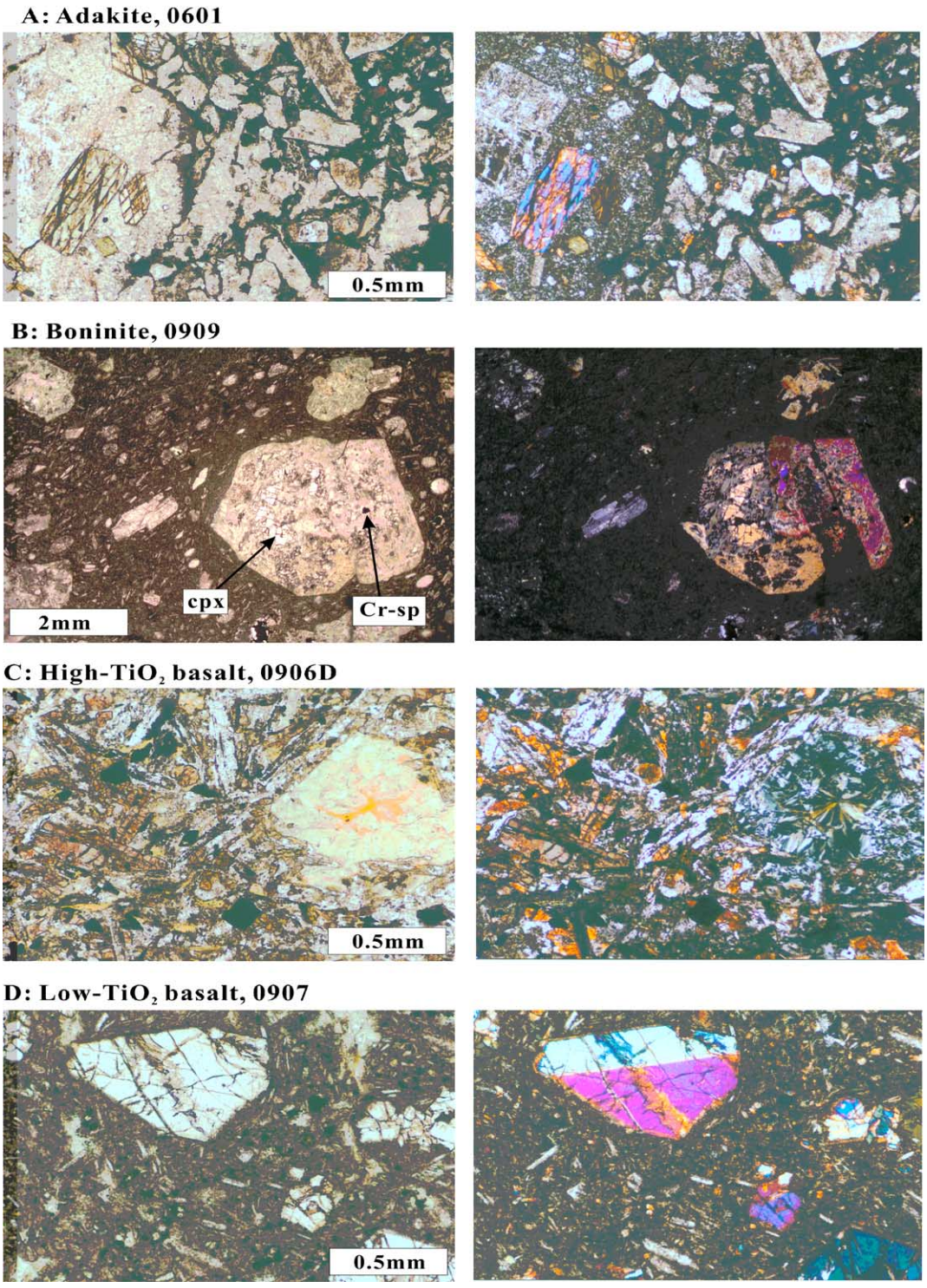

Fig. 2. Photomicrographs of some representative volcanic rocks. (A) adakite (0601a), Suoerkuduke area. The rock show clastic textures consisting of lithic fragments of hornblende andesite, pyroxene andesite, and crystal fragments of plagioclase, hornblende, augite, and apatite. (B) Boninite (0909B), Saebulake area. The rock is composed of metamorphic minerals of hornblende, epidote, carbonate, chlorite, plagioclase, and fine-grained matrix minerals. Relict augite and chromite are observed. (C) Low-TiO_2 basalt (0907), Saebulake area. Phenocrysts of augite and plagioclase are fresh set in a fine-grained matrix. (D) High-TiO_2 basalt (0906D), Saebulake area. Phenocrystal olivine is altered to serpentine, whereas, groundmass plagioclase, Ti-augite, titanomagnetite and ilmenite are fresh. Interstitial glass is altered.

Altay, are metamorphosed, but retain their porphyritic texture. Phenocryst minerals include olivine, augite, and plagioclase. Olivine shows idiomorphic crystal outlines, range in size from 0.2 to 1 mm long, and constitutes ca. 3–5 vol% of the rock. Olivine is completely altered to serpentine minerals. Augite constitutes ca. 5 vol% of the rock, and is 0.3–3 mm long. It is mostly altered to hornblende, epidote, chlorite, and carbonate, but locally fresh augite is preserved in some grains (Fig. 2B).

Table 1
Representative analyses of minerals in the Altay adakite, boninite and peridotite

Sample no.	0601		0909					1304			
rock	adakite		boninite					peridotite			
phase	hb	hb	cp	cp	cp	sp	sp	ol	ol	sp	Sp
point no.	hb-1-6	hb-1-13	cp-32	cp	cp	cp-1-27	cp-1-26	ol-52	ol-66	chr-19	chr-33
SiO_2	48.18	42.63	55.22	54.97	54.33	0.00	0.06	41.25	41.41	0.36	0.03
TiO_2	0.77	0.86	0.04	0.02	0.05	0.15	0.23	0.00	0.00	0.38	0.13
Al_2O_3	8.21	13.63	0.53	0.68	1.16	7.14	7.31	0.01	0.00	6.22	20.95
Cr_2O_3	0.01	0.03	0.54	0.60	0.63	56.40	54.68	0.00	0.00	49.94	41.46
FeO	12.32	16.98	2.55	2.93	3.75	27.50	28.97	10.21	9.79	37.30	29.22
MnO	0.48	0.38	0.14	0.07	0.12	0.63	0.70	0.06	0.16	0.63	0.55
NiO	–	–	0.04	0.05	0.00	0.05	0.07	0.38	0.39	0.05	0.06
MgO	14.81	9.70	19.01	18.37	18.59	7.83	7.97	48.50	49.91	4.14	7.85
CaO	10.88	11.05	22.85	22.75	21.99	0.03	0.04	0.01	0.01	0.02	0.03
Na_2O	1.21	1.83	0.07	0.13	0.13	0.03	0.02	0.01	0.05	0.00	0.22
K_2O	0.31	0.98	0.02	0.00	0.04	0.03	0.01	0.01	0.02	0.01	0.04
Total	97.16	98.06	100.98	100.58	100.78	99.78	100.06	100.44	101.75	99.03	100.53
O	23	23	6	6	6	4	4	4	4	4	4
Si	7.020	6.371	1.981	1.983	1.962	0.000	0.002	1.008	0.998	0.013	0.001
Al	1.409	2.401	0.022	0.029	0.049	0.285	0.291	0.000	0.000	0.257	0.784
Ti	0.085	0.097	0.001	0.001	0.001	0.004	0.006	0.000	0.000	0.010	0.003
Cr	0.001	0.004	0.015	0.017	0.018	1.513	1.459	0.000	0.000	1.387	1.041
Fe^{+3}			–	–	–	0.193	0.233	–	–	0.310	0.162
Fe^{+2}	1.501	2.122	0.076	0.088	0.113	0.588	0.584	0.209	0.197	0.786	0.614
Mn	0.059	0.048	0.004	0.002	0.004	0.018	0.020	0.001	0.003	0.019	0.015
Ni	3.217	2.160	0.001	0.001	0.000	0.001	0.002	0.008	0.008	0.001	0.001
Mg	0.000	0.000	1.017	0.988	1.000	0.396	0.401	1.766	1.794	0.217	0.372
Ca	1.699	1.769	0.878	0.879	0.850	0.001	0.002	0.000	0.000	0.001	0.001
Na	0.340	0.529	0.005	0.009	0.009	0.002	0.001	0.000	0.002	0.000	0.014
K	0.057	0.186	0.001	0.000	0.002	0.001	0.000	0.000	0.001	0.000	0.002
Total	15.388	15.688	4.002	3.998	4.009	3.002	3.001	2.992	3.003	3.000	3.010
Mg/(Mg+Fe)	0.682	0.504	0.930	0.918	0.898	0.403	0.407	0.894	0.901	0.216	0.377
Cr/(Cr+)	–	–	0.409	0.372	0.268	0.841	0.834	–	–	0.843	0.570

Abbreviation: hb, hornblende; cp, clinopyroxene; sp, spinel; ol, olvine.

Dark brown chromian spinel (0.1–0.3 mm) is often included in augite phenocrysts (Fig. 2B). Plagioclase ranges from 0.2 to 1 mm in length, and altered to carbonate, but is distinguished by its idiomorphic outline, and shadow of concentric zoning. It constitutes ca. 5 vol% of the rock. The groundmass shows hyalopilitic texture, which is too fine grained to identify the mineral constituents. Some of ovoidal vesicles are filled with carbonate.

Representative analyses of original minerals are listed in Table 1. The Mg/(Mg+Fe) ratios of augite cores range from 0.90 to 0.92, and Cr_2O_3 contents range from 0.5 to 0.7 wt%. The low content of TiO_2 in augite (<0.1 wt%) is consistent with the low TiO_2 contents of the host rock, and is characteristic of boninite. Relict chromian spinel included in a augite phenocryst have extremely high Cr/(Cr+Al) ratios (0.82–0.84) comparable to those of boninite from the Bonin Islands (Shiraki et al., 1980).

3.3. High-TiO_2 basalt and gabbro

High-TiO_2 basalt and gabbro contain 1.7–3.1 wt% TiO_2. They occur in the Suoerkuduke, Saerbulake, and Kuerti areas. High-TiO_2 basalts of the Kuerti area were suffered from regional metamorphism, and the constituent minerals are hornblende, epidote, calcite, sphene, magnetite, albite, and apatite. High-TiO_2 basalts of Suoerkuduke and Saerbulake were little affected by metamorphism, and retain their original textures. They are mostly aphyric to sparsely-phyric, with sporadic phenocrysts of olivine (altered to serpentine or carbonate) and plagioclase (partly altered to clay minerals or mica). The groundmass consists of Ti-augite, magnetite, ilmenite, plagioclase, apatite, and interstitial mesostasis, which is altered to clay minerals, chlorite and carbonate (Fig. 2C). High-TiO_2 gabbro is found only in the Saerbulake area, where it is associated with high-TiO_2 basalts, low-TiO_2 basalts, and low-TiO_2 gabbros. The gabbro consists of olivine (altered to clay/serpentine), augite, plagioclase, magnetite, apatite, and interstitial materials (altered to clay minerals, chlorite, and carbonate).

3.4. Low-TiO_2 basalt and gabbro

Low-TiO_2 basalt contains 0.3–1.5 wt% TiO_2, and is the main rock type in the Suoerkuduke, Saerbulake, and Ashele

areas. Low-TiO_2 basalt in the Ashele area is metamorphosed to greenschist facies, although the original texture is retained. The basalt is sparsely phyric, consisting of some phenocrysts now completely replaced by carbonate, chlorite, and epidote, with intergranular groundmass composed of epidote, chlorite, plagioclase and oxide minerals. Low-TiO_2 basalts of the Suoerkuduke and Saerbulake areas are less altered (Fig. 2D) and composed of sporadic phenocrysts of plagioclase, augite (often altered to carbonate) and olivine (altered to chlorite or clay minerals), with a groundmass consisting of plagioclase, augite, iron-oxides, and altered mesostasis. A low-TiO_2 gabbro was found in Suorkuduke, and consists of plagioclase (partly altered to clay), augite, olivine (completely altered to clay), magnetite, apatite, and interstitial minerals altered to clay.

3.5. Peridotite

Peridotite was only identified in the Kekesentao area. It consists of coarse-grained olivine, chromian spinel, with secondary serpentine, tremolite, and iron oxides. The Mg/(Mg + Fe) ratios of olivine are mostly 0.89–0.90, and the Cr/(Cr + Al) ratios of chromian spinel range from 0.56 to 0.79, mostly in the range of 0.56–0.60 (Table 1). These compositions of olivine and chromian spinel indicate that the peridotite represents a mildly-depleted mantle peridotite (Arai, 1994).

3.6. Gneiss, granites and diorites

Gneissose granite occurs in the middle of the Kuerti section, where the granite divides the northeastern and southwestern sections of green rock and layered sequence. Zircon grains in the granite were used for U/Pb chronometry, giving an age of 372 ± 19 Ma (Zhang et al., 2003). The rock is coarse-medium grained, and composed of plagioclase, quartz, alkali feldspar, biotite, hornblende, sphene, zircon, Fe–Ti oxides, apatite, and allanite. Myrmeckitic texture is commonly found. Fine-grained diorite (#1110 in Table 2) occurs in the Ashele area. The diorite consists of plagioclase, hornblende, biotite, quartz, K-feldspar, chlorite, epidote, and apatite.

3.7. Other volcanic rocks

Other volcanic rocks include quartz porphyry in the Ashele area and dacite in the Kekesentao area. The quartz porphyry (#1104, #1107) contains phenocrysts of quartz, plagioclase (partly altered to carbonate and chlorite) and mafic minerals (completely altered to oxides, carbonate, muscovite, and chlorite). The groundmass consists of fine-grained quartz, feldspars, oxides, and substantial amounts of secondary carbonate and chlorite. The dacite of Kekesentao (#1310) represents a welded tuff deposit, showing eutaxitic texture in the matrix. Phenocryst phases are generally unaltered and include biotite, hornblende, orthopyroxene, augite, iron oxides, quartz and plagioclase. The groundmass is glassy with microlites of feldspar and biotite.

4. Bulk rock chemistry

Bulk rock major and some trace element compositions were obtained by X-ray fluorescence spectrometry at Yamaguchi University, whereas trace element compositions and Sr, Nd isotopic compositions of some representative samples were obtained by ICP-MS and MCICP-MS at the Guangzhou Institute of Geochemistry, Chinese Academy of Science. The analytical methods and precisions were reported in Nagao et al. (1997), Li (1997), Xu et al. (2000) and Liang et al. (2003). The results are presented in Tables 2–4, and illustrated in SiO_2 variation diagrams in Fig. 3, and other geochemical diagrams in Figs. 4 and 5.

The adakitic rocks have high Sr/Y ratios of 120–136 and Y contents of 14–16 ppm. Although they show volcaniclastic texture, the rocks are mostly composed of poorly sorted angular rock fragments of hornblende andesite and pyroxene andesite together with crystal fragments of plagioclase, hornblende and pyroxene possibly representing a mixture of adakitic rocks. Slightly low SiO_2 contents (56.3 wt% on anhydrous basis) may be ascribed to the selective concentration of mineral phases in the volcaniclastic deposit. Plagioclase may have undergone albitization (Ab75-98). Other characteristics of the adakites are the very high contents of Ba (739–889 ppm), and Na_2O (4.9 wt%). Fig. 4 shows the chondrite-normalized REE patterns of adakite and boninites. The adakite shows enrichment in LREE with moderate depletion of HREE. Initial Sr isotopic compositions (0.70465–0.70489) and $\varepsilon_{Nd}(T)$ (+3.0 to +4.3) indicate slightly depleted characteristics, consistent with the derivation of the adakite from MORB-like source materials slightly contaminated by enriched components, such as subducted sediments.

The boninites have MgO contents of 8.4–9.4 wt% and Ni and Cr contents of 95–142, and 322–562 ppm, respectively. The SiO_2 (54.9–56.8 wt%) and CaO (10.2–8.9 wt%) contents are consistent with high-Ca boninite (Crawford et al., 1989). The Mg/(Mg + Fe) ratios of the bulk rock range from 0.65 to 0.68. The low TiO_2 (0.26–0.28 wt%) Zr and Y contents of the boninite indicate derivation from depleted mantle, which is consistent with the high Cr/(Cr + Al) ratio of chromian spinel in clinopyroxene phenocrysts. Fig. 4 demonstrates that boninites of Saerbulake area show a range of La/Yb ratios (1.8–8.6), although depleted in HREE. The low La/Yb boninites show slightly U-shaped REE patterns with negative Eu anomalies, whereas the high La/Yb boninites do not have significant Eu-anomalies. Initial Sr isotopic compositions and $\varepsilon_{Nd}(T)$ of the boninites are 0.7014–0.7052 and +6.6, respectively. These values are similar to those of boninites from Bonin Island (Taylor et al., 1994)) and other localities (Cameron et al., 1983).

Basalts can be classified into high-TiO_2 ($TiO_2 > 1.7$ wt%) and low-TiO_2 basalts ($TiO_2 < 1.5$ wt%) in SiO_2 variation diagrams (Fig. 3). TiO_2 is correlated with Y and Zr contents, and Ti/Y and Ti/Zr ratios (12–18 and 2.3–4.1, respectively) are similar to those of MORB and BABB samples. The Na_2O, K_2O and Rb contents of volcanic rocks of Altay are widely scattered in Fig. 3, suggesting that alkalis migrated and were affected by

Table 2
X-ray fluorescence analyses of major and trace elements of representative samples of the Devonian volcanic rocks of Altay area, Xinjiang, China

	1	2	3	4	5	6	7	8	9	10	11	12	13	14	15	16	17	18	19
Locality	Suoerkuduke																		
Sample No.	0601-(1)	0601-(2)	0604B	0604C	0605	0610	0611	0612	0708	0709	0801	0807	0902	0904	0906A	0906B	0906C	0906D	0906E
Latitude	46°31.55′	46°31.55′	46°31.91′	46°31.91′	46°31.88′	46°30.00′		46°28.07′	47°09.90′	47°10.02′	47°08.71′	47°06.91	46°51.48′	46°55.15′	46°54.90′	46°54.90′	46°54.90′	46°54.90′	46°54.90′
Longitude	89°34.64′	89°34.64′	89°34.62′	89°34.63′	89°34.55′	89°41.47′		89°39.57′	89°16.95′	89°17.05′	89°15.63′	89°13.66’	89°24.61′	89°27.56′	89°16.12′	89°16.12′	89°16.12′	89°16.12′	89°16.12′
Rock name	Adakite	Adakite	Basalt	Basalt	Basalt	Basalt	Andesite		Amphi-bolite	Granite	Psamitic Schist	Amphi-bolite	Shale	Sand-stone	Alkali basalt	Basalt	Dolerite	Basalt	Basalt
Occur-rence	vc	vc	m. lava	m. lava	m. lava	tuff	m. lava	Tuff											
SiO2	55.12	55.16	53.81	51.90	50.86	49.47	62.06	32.13	49.27	76.55	70.32	49.56	55.10	61.98	47.43	47.96	47.73	47.17	52.34
TiO2	0.77	0.77	1.04	1.78	0.96	1.06	0.48	2.27	3.02	0.26	0.39	2.31	0.71	0.72	2.84	2.57	2.07	2.66	0.71
Al2O3	18.23	18.26	16.11	16.18	15.97	16.27	16.40	7.70	12.59	11.93	15.24	13.44	18.90	17.00	15.80	15.43	17.25	14.97	13.02
Fe2O3	8.12	8.12	11.86	9.98	12.32	13.56	5.65	13.16	14.19	1.72	3.30	12.57	7.36	6.50	13.53	12.72	10.74	12.85	8.05
MnO	0.14	0.14	0.21	0.15	0.15	0.15	0.09	0.41	0.24	0.04	0.08	0.21	0.18	0.10	0.22	0.17	0.16	0.20	0.18
MgO	3.59	3.55	2.93	4.44	4.25	6.34	3.72	5.17	6.36	0.22	0.95	6.26	2.98	2.72	5.38	6.04	6.37	5.72	9.45
CaO	5.18	5.17	4.76	7.48	4.28	5.56	2.05	22.94	10.00	0.74	2.88	11.04	2.38	2.86	5.66	5.79	8.04	6.77	6.73
Na2O	4.92	4.89	6.42	2.95	5.36	3.24	4.63	0.79	3.26	4.20	4.72	2.69	7.38	3.99	4.94	5.07	3.63	4.93	5.70
K2O	1.70	1.70	0.82	1.69	1.47	0.30	1.15	0.61	0.32	3.53	2.06	0.28	1.53	1.85	0.52	0.22	1.18	0.34	0.13
P2O5	0.21	0.21	0.44	0.70	0.27	0.22	0.15	0.17	0.32	0.08	0.10	0.20	0.45	0.15	0.45	0.45	0.24	0.51	0.15
Total	97.97	97.97	98.40	97.24	95.87	96.15	96.39	85.34	99.55	99.26	100.03	98.57	96.97	97.87	96.76	96.42	97.4	96.12	96.46
FeO/MgO	2.04	2.06	3.64	2.02	2.61	1.93	1.37	2.29	2.01	7.12	3.14	1.81	2.22	2.15	2.26	1.90	1.52	2.02	0.77
Ba	741	738	180	604	711	169	196	332	59.1	223	418	114	243	302	36	18	127	14.7	34
Co	26.4	25.9	30.1	29.5	31.6	38.9	11.7	36.4	46.2	53.2	8.7	41.1	8.9	17.8	44.1	46.6	42.6	46.1	42.7
Cr	27.5	28.9	6.7	71.4	14.2	83.4	30.3	313	93.5	5.4	8	283	10.6	32.9	91.8	73.3	130	84.3	521
Cu	48.3	47.2	371	0.6	264	63	67.8	215	18.6	6.6	10.6	25.9	53.5	42.6	44.5	36	60.4	33.1	0
Ga	19.7	20.1	19.4	18	14.4	20	15.1	13	14.4	13	15.8	16.9	17	16.9	19.7	16.7	18.8	20.9	12.1
Nb	4.46	4.91	4.61	17.2	2.82	4.74	4.86	12.3	8.69	15.6	5.73	5.04	5.53	5	9.96	8.62	4.71	10.2	2.08
Ni	10.4	10.7	3.1	14.5	11.5	23.9	30.1	35.4	41	5.9	4.6	54.9	1.8	14.4	47.6	68.3	54.3	60.9	241
Pb	6.19	6.13	5.67	6.51	3.48	3.44	2.22	3.06	0.9	18.8	15.2	2.88	24.7	7.27	1.98	0	1.1	0.3	1.87
Rb	30.7	31.1	7.2	14.9	15.3	4.7	22.3	6.3	1.2	124	73.3	2	17.4	39.4	7.6	4	21.4	8.2	3.5
Sr	1910	1908	493	751	964	653	383	328	198	59.7	165	197	341	379	565	410	515	462	176
Th	3.74	7.15	7.89	7.95	4.25	4.65	4.92	0.74	<0.1	21.7	9.59	0.1	6.09	3.8	3.25	3.87	n.d.	1.39	4.35
V	228	230	220	182	348	371	105	514	417	16.4	37.6	384	107	139	222	191	268	197	212
Y	15.8	14.1	31.9	41.4	20.2	19.5	10.6	40.4	47	43.2	24.6	44.8	24.6	20.4	58.7	54.8	39.5	60.2	16.2
Zn	86.9	87.8	99.6	103	109	119	63.6	145	121	29.6	54.4	87	153	75.8	103	91.8	73.7	94.1	56.3
Zr	89.4	89.5	116	314	80.1	76.1	79.5	111	200	215	142	150	98.6	125	336	303	175	338	71
Sr/Y	121	135	15.4	18.1	47.7	33.5	36.1	8.1	4.2	1.4	6.7	4.4	13.9	18.6	9.6	7.5	13.0	7.7	10.9
Sr/Rb	62.2	61.4	68.4	50.4	63.0	139	17.2	52.1	165	0.5	2.3	98.5	19.6	9.6	74.3	103	24.1	56.3	50.3
	20	21	22	23	24	25	26	27	28	29	30	31	32	33	34	35	36	37	38

Table 2 (*continued*)

Locality	Saerbu-lake																	Ashele	
Sample No.	0906F	0906H-(1)	0906H(-4)	0906I	0906J	0906K	0906L-1	0906L-2	0906M	0906N	0906O-1	0906O-2	0907	0908	0909A	0909B	0910	1101	1103
Latitude	46°54.90′	46°54.90′	46°54.90′	46°54.90′	46°54.90′	46°54.90′	46°54.90′	46°54.90′	46°54.90′	46°54.90′	46°54.90′	46°54.90′	46°55.23′	46°55.24′	46°55.22′	46°55.22′	46°55.20′	48°18.06′	48°17.71′
Longi-tude	89°16.12′	89°16.12′	89°16.12′	89°16.12′	89°16.12′	89°16.12′	89°16.12′	89°16.12′	89°16.12′	89°16.12′	89°16.12′	89°16.12′	89°15.77′	89°16.06′	89°16.03′	89°16.03′	89°15.87′	86°20.68′	86°20.58′
Rock name	Gabbro	Basalt	Basalt	Basalt	Basalt	Gabbro	Andesite	Andesite	Sand-stone	Basalt	Dolerite	Dolerite	Basalt	Basalt	Boninite	Boninite	Basalt	qz-por-phyry	Altered and.
Occur-rence					Lapilli tuff		Tuff	Tuff		Lava									
SiO2	46.77	48.93	49.06	46.65	47.82	50.31	54.73	54.51	53.52	49.81	46.32	46.52	50.04	47.45	54.94	56.84	47.54	64.33	50.89
TiO2	3.04	0.36	0.35	0.31	0.74	1.44	0.48	0.48	0.84	2.31	2.22	2.22	0.51	0.46	0.28	0.26	0.55	0.29	0.58
Al2O3	14.64	18.69	18.86	18.18	14.47	15.44	18.11	18.34	15.67	16.25	16.94	17.04	15.13	17.78	11.16	10.54	17.69	14.21	13.56
Fe2O3	12.14	8.01	8.01	8.17	9.17	12.85	5.40	5.45	6.81	11.70	11.67	11.72	9.20	9.89	8.10	8.06	9.48	5.84	10.77
MnO	0.16	0.11	0.11	0.14	0.14	0.21	0.12	0.12	0.12	0.16	0.17	0.17	0.16	0.17	0.18	0.17	0.17	0.11	0.07
MgO	5.23	6.28	6.30	5.84	10.70	5.71	1.85	1.77	5.17	3.92	7.15	7.22	8.19	7.94	8.44	9.42	7.47	2.20	4.07
CaO	11.12	8.11	8.14	12.68	8.16	6.34	12.23	12.64	8.15	6.26	8.35	8.37	8.74	8.52	10.17	8.87	8.69	4.70	7.84
Na2O	4.14	2.10	2.08	2.28	4.06	4.86	3.79	3.54	6.02	5.58	3.49	3.47	2.94	1.30	2.07	1.60	3.04	3.70	4.84
K2O	0.13	3.22	3.21	1.83	0.16	0.56	0.11	0.12	0.27	0.38	0.85	0.85	2.02	3.19	2.62	2.48	1.43	0.65	0.66
P2O5	0.27	0.20	0.21	0.21	0.14	0.12	0.14	0.14	0.33	0.64	0.30	0.31	0.21	0.19	0.35	0.18	0.22	0.03	0.07
Total	97.63	95.99	96.32	96.28	95.55	97.85	96.96	97.13	96.89	97.00	97.45	97.88	97.13	96.90	98.32	98.42	96.27	96.05	93.35
FeO/MgO	2.09	1.15	1.14	1.26	0.77	2.02	2.63	2.77	1.19	2.68	1.47	1.46	1.01	1.12	0.86	0.77	1.14	2.39	2.38
Ba	78.6	254	272	157	42.3	132	35	43.6	55.4	127	87.6	75.7	367	541	1107	1311	260	92.6	63.6
Co	41.5	35.5	37.4	34.8	49.1	48	14.2	14.2	29.4	27.6	49.2	49.6	42.3	43.7	37.4	38.5	42.4	16.1	34.5
Cr	84.5	196	197	218	629	5.6	66.5	66.9	286	14.3	129	131	310	148	322	563	108	10.8	226
Cu	159	2372	2347	96.4	69.1	194	<0.1	<0.1	50.2	39.9	47.2	48.2	83.9	118	55.6	49.6	114	29.7	19.5
Ga	18.6	12.1	12	11.2	15.6	15.1	15.7	17.8	15.2	22.8	19.3	18.4	11.3	11.6	8.7	6.2	12.7	11.5	10.1
Nb	5.32	2.62	1.63	1.83	3.19	1.73	3.92	3.43	3.83	9.08	5.96	6.59	2.06	3.63	1.77	1.33	2.1	1.79	1.84
Ni	23.4	64.4	63.9	61.9	290	19.7	24.8	23.7	88.5	6.2	75.6	81.9	80.1	56.7	94.8	142	45.1	6.4	70.3
Pb	0	1.41	1.8	1.4	1.37	0	4.44	4.59	4.24	<0.1	<0.1	0.43	1.71	<0.1	1.93	n.d.	2.27	2.89	n.d.
Rb	0	65.7	62.4	30	2.8	8.3	2.3	3.3	5.3	6.3	13.6	11.8	32.2	47.9	41	40.2	24.1	12	15.1
Sr	252	460	455	202	244	412	3163	3316	380	556	532	535	449	279	290	260	449	138	122
Th	n.d.	4.56	4.1	2.49	4.29	0.85	1.18	4.09	3.52	5.36	0.65	0.9	4.05	1.44	0.21	0.24	1.23	4.92	5.34
V	414	193	194	133	236	312	183	193	264	177	239	240	238	288	226	235	224	120	251
Y	43.1	10.6	12.1	8.1	18.3	34.7	11.1	9.2	21.8	74.8	41.4	40.2	13.1	13.1	10	9.1	11.3	16.8	8.9
Zn	72.8	60.7	61.9	50.6	73.3	98.9	35.1	35.4	47.2	113	78.2	77.9	64.8	65.1	62.5	62.2	82.6	56.7	58.6
Zr	234	21.8	21.2	17.9	77.4	96.5	43.8	45.6	89.1	443	253	258	25.8	24.3	22.3	18.3	18.6	47.3	32.5
Sr/Y	5.8	43.4	37.6	24.9	13.3	11.9	285	360	17.4	7.4	12.9	13.3	34.3	21.3	29.0	28.6	39.7	8.2	13.7
Sr/Rb	–	7.0	7.3	6.7	87.1	49.6	1375	1005	71.8	88.2	39.1	45.3	13.9	5.8	7.1	6.5	18.6	11.5	8.1
	39	40	41	42	43	44	45	46	47	48	49	50	51	52	53	54	55		

Locality	Ashele											Kakesen-tao					
Sample No.	1103	1104	1105	1107	1110	1111	1201	1202	1203	1206	1207	1301	1304	1305	1306	1309	1310
Latitude	48°17.71′	48°17.60′	48°17.51′	48°17.73′	48°17.00′	48°16.91′	48°19.35′	48°19.38′	48°19.38′	48°19.02′	48°18.88′	47°36.81′	47°35.53′	47°35.49′	47°35.47′	47°35.68′	47°35.68′
Longitude	86°20.58′	86°20.61′	86°20.33′	86°20.20′	86°21.36′	86°21.06′	86°20.60′	86°20.58′	86°20.43′	86°20.23′	86°20.20′	86°34.59′	86°38.43′	86°38.40′	86°38.35′	86°38.56′	86°38.56′
Rock name	Altered and	qz-por-phyry	Basic schist	qz-por-phyry	Tonalite	Metaba-salt	Metaba-salt	Metaan-desite	Metaba-salt	Basalt	Basalt	Grano-diorite	Peridotite	Hornfels	Sandstone	Diorite	Dacite
											Lapilli tuff						Welded tuff
SiO2	50.46	65.46	46.23	71.18	58.12	50.36	50.79	60.11	51.53	49.17	51.66	66.70	42.06	76.50	76.20	52.62	67.91
TiO2	0.63	0.28	0.57	0.31	0.95	0.62	1.12	1.05	1.03	1.06	1.07	0.61	0.01	0.49	0.47	0.94	0.60
Al2O3	13.97	13.70	13.26	12.56	16.10	14.44	15.82	15.35	17.31	15.36	17.71	15.44	0.67	10.47	11.99	15.69	15.66
Fe2O3	8.30	5.36	9.53	3.96	7.15	15.51	13.54	5.77	11.20	11.54	10.00	4.80	10.09	4.11	2.94	8.26	4.21
MnO	0.08	0.04	0.15	0.08	0.13	1.05	0.18	0.10	0.16	0.15	0.16	0.12	0.12	0.11	0.05	0.16	0.08
MgO	4.45	2.42	9.66	0.70	3.45	5.15	5.27	3.85	5.65	5.70	4.46	2.87	41.96	2.49	1.35	7.68	1.13
CaO	9.54	3.80	7.88	2.28	5.62	9.24	8.66	5.06	5.42	5.57	7.79	3.13	0.78	0.33	1.11	6.94	2.79
Na2O	4.88	4.05	1.96	5.47	3.79	0.03	1.16	4.50	4.90	4.39	3.32	3.02	0.04	1.47	3.44	2.19	3.86
K2O	0.34	0.66	0.08	0.56	2.57	0.00	0.00	0.19	0.01	0.00	0.00	2.50	n.d.	2.52	1.40	3.47	3.81
P2O5	0.09	0.04	0.06	0.05	0.52	0.03	0.13	0.32	0.11	0.11	0.13	0.13	0.00	0.07	0.10	0.10	0.19
Total	92.73	95.80	89.39	97.14	98.39	96.44	96.66	96.29	97.31	93.03	96.30	99.31	95.73	98.55	99.06	98.04	100.22
FeO/MgO	1.68	2.00	0.89	5.12	1.86	2.71	2.31	1.35	1.79	1.82	2.02	1.51	0.22	1.49	1.96	0.97	3.35
Ba	42.6	99.4	380	104	594	20	34.4	67.3	40.1	31.5	13.1	334	3.3	226	300	374	363
Co	38.6	27	44.2	11.1	22.8	44.8	40.5	21.4	39.4	39.8	28.9	17.6	129.1	10.7	8.8	31.7	10.5
Cr	255	15.1	303	5.3	78.3	17.2	48.5	69.6	39.3	105	39.2	70.4	2357	40.7	47	294	14.1
Cu	22.7	11.4	2.1	7.4	63.5	15.2	45.2	23.8	459	136	72.8	36.4	0.6	61.4	5.5	37.2	10.8
Ga	10.3	12.7	13.4	8.2	17.7	15.2	17.4	18.5	19.1	15.4	18.7	17.8	0.8	13.3	14	13.4	19
Nb	1.91	1.7	1.23	2.87	12.9	2.35	2.21	7.82	2.43	2.36	3.03	10.4	1.8	12.7	10.3	5.21	13.7
Ni	73.4	3	96.2	0.4	45	2.3	24.8	56.6	33.7	41.9	13.7	45.9	2292	15	19.1	114	8.2
Pb	1.84	3.48	7.65	5.55	20.6	10.5	4.46	8.26	2.27	n.d.	3.7	11.6	n.d.	12.0	17.9	6.38	18.1
Rb	8.7	12.2	3.4	13.2	39.2	0.3	2.3	9.9	0.9	1.5	2.4	89.5	n.d.	90.7	45.1	138	120
Sr	165	140	162	98.6	681	324	157	391	145	94.8	233	226	5.9	112	233	158	249
Th	4.01	5.85	4.49	8.67	4.59	8.61	3.9	5.22	2.82	2.74	1.24	6.91	n.d.	4.89	12.6	3.82	12.5
V	187	122	232	58.7	144	587	451	118	318	347	228	79.7	39.7	70.4	45.6	153	36.7
Y	8.7	12.4	11.1	29.3	25.2	12.1	22.6	18.6	25.4	23.7	24.5	25.8	3.8	18.5	25.1	27.1	34.1
Zn	64.1	50.8	67.8	43.5	115	494	107	77.8	108	88.3	92.1	69.5	45.9	65.3	42.2	69.8	65.2
Zr	33.9	44.4	29.9	82.7	231	21.6	44.9	114	51	44.3	76.6	166	6.9	129	216	102	246
Sr/Y	19.0	11.3	14.6	3.4	27.0	26.8	6.9	21.0	5.7	4.0	9.5	8.8	1.6	6.1	9.3	5.8	7.3
Sr/Rb	19.0	11.5	47.6	7.5	17.4	1081	68.3	39.5	161	63.2	97.1	2.5	–	1.2	5.2	1.1	2.1

Table 3
ICP-MS analyses of trace elements of boninite, adakite and related volcanic rocks of the Altay area, Xinjiang, China

Locality	Saerbu-lake														
Sample No.	0906	0906	0906	0906	0906	0906	0909	0909							
	BB06-1	BB06-7	BB06-8	BB06-9	BB-06-10	BB06-12	BB10-1	BB10-3	BB09-2	BB12-3	BB14-4	BB14-6	BB15-1	BB16	BB18-1
Latitude	89°16.12	89°16.12	89°16.12	89°16.12	89°16.12	89°16.12	89°16.03	89°16.03	89°16.00	89°16.00	89°16.23	89°16.23	89°16.12	89°17.94	89°18.37
Longitude	46°54.90	46°54.90	46°54.90	46°54.90	46°54.90	46°54.90	46°55.22	46°55.22	46°55.24	46°55.36	46°55.36	46°55.36	46°55.31	46°54.46	46°54.64
Rock type	Basalt	Basalt	Gabbro	Gabbro	Gabbro	Gabbro	Boninite	Boninite	Boninite	Boninite	Boninite	Boninite	Boninite	Boninite	Boninite
P	1145	642	2302	377	506	889	953	1480	825	652	1096	668	1814	1278	869
Sc	38.5	35.3	46.6	44.5	33.2	42.7	39.8	31.4	37.1	42.6	18.6	51.5	39.9	30.7	24.3
Ti	14311	4761	21587	21033	7529	17251	1829	1468	1476	2239	2129	2018	2181	1402	2090
V	274	242	297	495	273	539	195	189	201	209	123	275	250	215	168
Cr	125	1391	138	103	5	356	266	265	395	230	25	385	75	39	76
Mn	1294	1558	1507	1622	1427	2420	1252	1413	1230	1159	1041	1298	1107	795	1158
Co	37	64	38	56	42	40	33	29	45	37	27	36	24	19	18
Ni	54	523	25	59	22	43	105	77	111	68	31	69	31	29	31
Ga	19.5	15.8	22.7	16.8	16.3	13.1	8.7	7.9	6.4	12.3	12.4	10.6	12.9	11.3	11.1
Ge	1.72	1.54	2.12	1.62	1.57	2.09	1.83	1.76	1.71	1.58	1.08	1.73	1.52	1.16	1.81
Rb	19.3	1.47	7.23	11.3	10.1	5.33	45.2	28.5	30.2	23.8	23.4	20.9	24.9	44.9	22.0
Sr	526	147	471	420	398	234	300	242	131	688	516	170	685	791	597
Y	43.7	15.8	63.9	20.5	28.2	32.3	10.9	12.2	9.1	9.9	9.8	10.7	11.1	8.1	10.2
Zr	198	63	289	81	83	103	17	14	13	20	34	16	17	12	27
Nb	3.93	1.45	8.12	1.57	0.61	11.49	0.87	0.70	0.70	3.05	5.71	1.15	2.33	2.70	3.10
Cs	0.50	0.09	0.57	0.64	0.37	0.14	0.70	0.32	0.16	2.17	0.60	0.44	0.21	0.88	0.24
Ba	90	25	53	41	100	169	1573	732	1511	393	652	763	562	894	651
La	7.34	7.55	16.20	3.39	3.61	20.06	2.27	2.53	1.85	2.24	4.63	1.79	10.72	5.74	5.65
Ce	22.2	18.3	46.2	10.0	11.3	42.7	4.83	5.30	4.00	4.89	8.83	3.94	21.3	9.66	11.4
Pr	3.70	2.79	7.35	1.76	2.02	5.82	0.67	0.74	0.55	0.69	1.12	0.56	2.88	1.14	1.44
Nd	18.8	13.4	36.4	9.47	11.2	26.3	3.17	3.40	2.61	3.17	4.73	2.73	13.0	4.49	6.12
Sm	5.41	3.33	9.43	2.89	3.50	5.99	0.89	0.95	0.70	0.89	1.13	0.80	2.51	0.89	1.39
Eu	2.002	1.030	3.072	1.284	1.286	1.951	0.137	0.241	0.145	0.335	0.342	0.232	0.688	0.241	0.408
Gd	6.91	3.38	11.21	3.89	4.84	6.41	1.61	1.49	1.28	1.38	1.59	1.35	2.26	1.13	1.65
Tb	1.168	0.508	1.873	0.620	0.791	0.963	0.234	0.241	0.201	0.239	0.239	0.226	0.324	0.168	0.254
Dy	6.99	2.75	10.96	3.95	5.17	5.81	1.56	1.62	1.32	1.54	1.52	1.55	1.79	1.13	1.60
Ho	1.42	0.54	2.27	0.79	1.07	1.15	0.36	0.37	0.30	0.33	0.33	0.35	0.37	0.27	0.34
Er	4.05	1.44	6.39	1.99	2.88	3.05	1.07	1.14	0.92	0.96	0.96	1.06	1.09	0.82	1.00
Tm	0.63	0.22	0.98	0.32	0.46	0.48	0.19	0.19	0.15	0.16	0.16	0.18	0.18	0.14	0.17
Yb	3.97	1.35	6.22	1.93	3.09	3.18	1.24	1.26	1.03	1.05	1.05	1.22	1.25	1.01	1.08
Lu	0.64	0.22	0.97	0.31	0.49	0.51	0.21	0.22	0.17	0.17	0.18	0.20	0.21	0.18	0.19
Hf	4.34	1.76	7.05	2.28	2.56	2.69	0.49	0.40	0.38	0.56	0.84	0.47	0.61	0.39	0.76
Ta	0.265	0.079	0.576	0.137	0.048	0.565	0.064	0.051	0.050	0.177	0.346	0.077	0.137	0.158	0.185
Th	0.46	0.85	0.75	0.16	0.53	1.15	0.33	0.26	0.28	0.29	0.76	0.22	1.38	0.58	0.81
U	0.20	0.45	0.35	0.08	0.18	0.48	0.59	0.56	0.26	0.10	0.46	0.14	0.65	0.34	0.33
Sr/Y	12	9	7	20	14	7	27	20	14	69	52	16	62	98	58

Locality	Suoerku-duke	Ashele						Kekesentao					
Sample No	0601	1101	1105	1110	1202	1203	1206	1302	1304				
	A01-1	BA01	BA06-5	BA11-1	BA14-1	BA17	BA19-2	OK-2	OK03-2	OK-4	OK-5	OK10-1	OK15-2
Latitude	46°31.55	86°20.68	86°20.33	86°21.36	86°20.58	86°20.43	86°20.30	86°38.62	86°38.44	86°38.40	86°38.35	86°38.48	86°38.56
Longitude	89°34.64	48°18.06	48°17.51	48°17.00	48°19.38	48°19.38	48°19.26	47°35.74	47°35.55	47°35.48	47°35.47	47°35.49	47°35.68
Rock type	Adakite	Dacite	Basic schist	Diorite	Diorite	Basalt	Basalt	Basalt	Peridotite	Hornfels	Sandstone	Granite	Pyroclastic Rock
Occurrence													
P	1096	146	380	2656	1205	429	553	374	33	181	567	242	860
Sc	16.8	32.5	24.0	16.3	13.2	33.1	40.4	39.5	9.2	10.1	9.2	3.3	9.8
Ti	5427	1916	4279	6176	5466	5415	6736	5665	49	2583	3274	2896	3614
V	285	151	241	130	111	268	369	241	53	57	53	25	36
Cr	26	10	352	84	56	36	59	370	2528	33	55	7	23
Mn	1276	722	899	982	667	1153	821	1256	311	1733	502	120	648
Co	38	16	42	21	18	29	30	39	193	11	5	4	7
Ni	15	3	101	45	51	31	34	131	2382	28	21	14	6
Ga	20.0	13.7	14.2	18.1	17.8	14.3	15.6	14.6	0.7	14.3	17.4	11.6	20.6
Ge	1.70	1.60	1.46	1.45	1.21	0.78	1.22	1.66	1.22	1.87	1.57	0.79	1.84
Rb	2.67	13.24	0.05	34.83	5.42	0.06	0.23	6.03	0.07	66.91	73.62	58.84	116.40
Sr	2045	119	112	533	412	69	112	124	3	62	125	232	233
Y	9.8	16.0	6.2	24.8	17.5	21.8	25.2	21.2	0.1	17.9	28.8	27.1	30.7
Zr	101	41	29	246	114	41	50	49	0	120	211	281	263
Nb	3.56	0.98	0.59	12.65	7.23	1.06	1.26	4.19	0.03	8.39	12.79	8.24	12.76
Cs	0.21	0.81	0.21	0.77	0.31	0.00	0.01	0.57	0.09	4.41	2.63	0.31	6.27
Ba	889	94	14	601	82	11	13	45	6	217	400	349	366
La	16.92	4.17	1.99	32.71	15.34	4.17	4.94	3.08	0.07	17.31	29.96	46.09	25.26
Ce	33.19	9.02	4.96	68.88	33.98	10.25	12.75	8.29	0.17	43.17	63.91	93.84	56.14
Pr	3.48	1.23	0.77	8.81	4.45	1.51	1.90	1.30	0.021	4.33	7.91	10.10	7.21
Nd	15.64	5.50	3.57	34.87	18.07	7.60	9.43	6.69	0.083	16.56	30.47	35.08	29.16
Sm	3.24	1.46	0.95	6.63	3.61	2.27	2.80	2.08	0.02	3.09	5.97	5.44	6.12
Eu	0.916	0.499	0.300	1.658	1.032	0.719	0.904	0.738	0.008	0.634	0.958	0.875	1.014
Gd	3.10	2.10	1.12	5.87	3.59	3.10	3.75	3.00	0.016	2.91	5.15	4.56	5.81
Tb	0.444	0.379	0.179	0.848	0.558	0.540	0.642	0.528	0.004	0.478	0.870	0.735	0.935
Dy	2.63	2.62	1.17	4.78	3.32	3.35	4.05	3.28	0.02	2.83	4.86	4.41	5.66
Ho	0.52	0.59	0.25	0.92	0.63	0.72	0.86	0.69	0.004	0.58	0.96	0.92	1.12
Er	1.40	1.67	0.70	2.44	1.67	2.10	2.49	2.02	0.012	1.76	2.86	2.75	2.98
Tm	0.23	0.29	0.11	0.39	0.27	0.33	0.41	0.31	0.002	0.29	0.46	0.45	0.49
Yb	1.48	2.02	0.77	2.46	1.72	2.19	2.63	2.07	0.021	1.93	3.05	3.06	3.22
Lu	0.24	0.34	0.13	0.39	0.27	0.35	0.42	0.33	0.004	0.32	0.49	0.54	0.52
Hf	2.91	1.39	0.97	5.72	3.16	1.27	1.57	1.29	0.010	3.18	5.82	8.04	6.96
Ta	0.222	0.086	0.053	0.712	0.555	0.068	0.082	0.250	0.007	0.571	1.002	0.706	1.285
Th	1.71	1.60	0.62	2.89	3.76	0.76	0.95	0.31	0.013	6.58	14.54	20.59	10.20
U	1.27	0.49	0.14	0.73	1.13	0.26	0.32	0.11	1.95	1.28	3.58	2.26	4.37
Sr/Y	209	7	18	21	24	3	4	6	21	3	4	9	8

Table 4
Isotope analyses of volcanic rocks of the Altay area, Xinjiang, China

Sample no.	Rock	Locality	Longitude	Latitude	Rb	Sr	$^{87}Rb/^{86}Sr$	$^{87}Sr/^{86}Sr$	2sigma SE	$(^{87}Sr/^{86}Sr)_0^*$	Sm	Nd	$^{143}Sm/^{144}Nd$	$^{143}Nd/^{144}Nd$	2sigma SE	$(^{143}Nd/^{144}Nd)_0^*$	$(^{143}Nd/^{144}Nd)_{CHUR}$	$\varepsilon_{Nd}(T)$
0906	BB06-1	Basalt	Saer-	46°54.90	89°16.12	19.31	526.1	0.1062	0.706746	0.000016	0.706617	5.407	18.8	0.173890	0.512989	0.000009	0.51257	0.512159	8.0
0906	BB06-7	Basalt	bulake	46°54.90	89°16.12	1.47	147.4	0.0288	0.705444	0.000018	0.70529	3.331	13.36	0.150741	0.512887	0.000008	0.51252	0.512159	7.1
0906	BB06-8	Gabbro		46°54.90	89°16.12	7.226	471.0	0.0444	0.704935	0.000018	0.70469	9.426	36.4	0.156571	0.513086	0.000010	0.51271	0.512159	10.7
	BB09-2	Boninte		46°55.24	89°16.00	30.21	130.7	0.6686	0.705058	0.000018	0.70142				–	–			
0909	BB10-3	Boninte		46°55.22	89°16.03	28.48	242.2	0.3402	0.707000	0.000040	0.70515	0.945	3.399	0.168092	0.512905	0.000009	0.51250	0.512159	6.6
	BB15-2	Bonnitic andesite		46°55.31	89°16.12	0.025	639.8	0.0001	0.704646	0.000013	0.70465				–	–			
	BB18-1	Boninitic andesite		46°54.64	89°18.37	22.00	596.9	0.1066	0.705112	0.000011	0.70453				–	–			
0601	A01-2	Adakite	Suoer-	46°31.55	89°34.64	25.48	1812.8	0.0407	0.704988	0.000016	0.70477	3.987	19.11	0.126133	0.512683	0.000011	0.51238	0.512159	4.3
	A03-2	Adakite	kudu-	46°31.70	89°34.61	18.82	1050.1	0.0518	0.705177	0.000016	0.70489	3.665	17.37	0.127561	0.512676	0.000011	0.51237	0.512159	4.1
	A06-3	Adakite	ke	46°32.59	89°34.55	16.26	503.3	0.0935	0.705154	0.000017	0.70465	4.277	20.2	0.128005	0.512624	0.000010	0.51231	0.512159	3.0
	A10-2	Adakite		46°30.00	89°41.47	13.40	720.3	0.0538	0.705079	0.000018	0.70479	3.507	16.76	0.126503	0.512644	0.000009	0.51234	0.512159	3.5
	A04-2	Nb-enriched basalt		46°31.90	89°34.62	22.04	694.6	0.0918	0.704435	0.000017	0.70394	14.44	69.07	0.126393	0.512713	0.000009	0.51241	0.512159	4.8
	A05-1	Nb-enriched basalt		46°31.88	89°34.55	26.50	684.5	0.1120	0.704519	0.000018	0.70391	14.04	68.1	0.124643	0.512730	0.000008	0.51243	0.512159	5.3

*Initial ratios of Sr and Nd isotopes are calculated for $t = 372$ Ma.

alteration, and may not be useful for geotectonic discrimination. Fig. 4B shows the chondrite-normalized REE patterns of basaltic rocks. Most of the basalts show slight enrichment in LREE, and high-TiO_2 basalts (solid symbols) generally contain higher abundances of total REE compared to low-TiO_2 basalts (open symbols). Fig. 5B illustrates the spider diagram for the low-TiO_2 basalts, which are classified into three different patterns. Four basalts obtained from the Saerbulake and Ashele areas are strongly depleted in Ta and Nb, with higher abundance ratios of Th (samples BA17, BB06-10, OK-2, BA19-2). One basalt from Kekesentao (sample BB06-7) has a flat pattern without any Nb and Ta depletion in Fig. 5B. Two samples from Kekesentao (sample OK-4 and OK-5) are more LIL enriched with mild depletions in HFS elements, and only minor depletion of Ta and Nb relative to Th and Ce. One low-TiO_2 basalt (BB06-7 in Table 4) shows slightly enriched Sr and depleted Nd isotopic compositions.

On the other hand, the spider diagrams of high-TiO_2 basalts and gabbros (Fig. 5A) illustrate more flat patterns commonly showing only minor Ta and Nb depletions between Th and Ce. One high-TiO_2 gabbro (BB06-9) illustrates no HFS enrichment relative to a MORB composition, but is enriched somehow in LIL elements. Other three high-TiO_2 basalts and gabbros show slightly convex upward patterns. These high-TiO_2 basalts are moderately depleted in Nd isotopic compositions ($\varepsilon_{Nd}(T) = 4.8–8.0$), reinforcing their MORB-, BABB- or OIB-like characteristics. One TiO_2-rich gabbro (BB06-8) is more like OIB in trace element pattern. The bulk rock composition of the peridotite in the Kekesentao area have low CaO (0.78 wt%), and Al_2O_3 (0.67 wt%) contents, and may be classified as enriched harzburgite-type ophiolites according to Ishiwatari (1985). This is consistent with the mineral chemistry of olivine ($Mg/(Mg+Fe) = 0.89–0.90$) and chromian spinel ($Cr/(Cr+Al) = 0.54–0.84$) as mildly depleted mantle peridotite (Arai, 1994).

5. Discussion

5.1. Origin of adakite and boninite

Adakite is characterized geochemically by high Sr/Y ratios with low Y and HREE contents, suggesting derivation from melting of subducted oceanic basalt in the garnet stability field (Defant and Drummond, 1990). In the southern Altay, adakite occurs in the Suoerkuduke area, and actually represents a fine-grained volcaniclastic deposit. The heterolithologic (hornblende andesite and pyroxene andesite) and poorly sorted nature of the rock suggest that the bulk rock most likely represents a mixed composition of a suite of andesites. Slight enrichment of plagioclase and mafic minerals are indicated from the Al_2O_3 (18.3 wt%) and MgO (5.2 wt%) contents. The rock has $SiO_2 = 55.1$ wt%, with very high Sr/Y ratios of 120–136 and low Y (14–16 ppm) and HREE (Fig. 4). Previous experimental studies indicate a more silicic composition of partial melts derived from subducted oceanic crust (Sen and Dunn, 1994; Rapp and Watson, 1995; Springer and Seck, 1997). The much

lower SiO_2 content of the Altay adakite may reflect interaction of the original adakitic melt with the overlying wedge mantle peridotite. This is consistent with the high MgO content of the adakite. Nd isotopic compositions ($\varepsilon_{Nd}(T) = +3.0$ to $+4.3$) are slightly depleted, which is interpreted as derivation from MORB-like material with some incorporation of sediments. The presence of adakite in the southern Altay area suggests the contribution of young slab melting in the formation of the continental crust.

The occurrence of boninite is mostly restricted to the fore-arc region, and its ultra-depleted geochemistry with slight enrichment of LIL elements suggest generation by partial melting of strongly depleted mantle peridotite by influx of slab derived aqueous fluid (Crawford et al., 1989; Shiraki et al.,

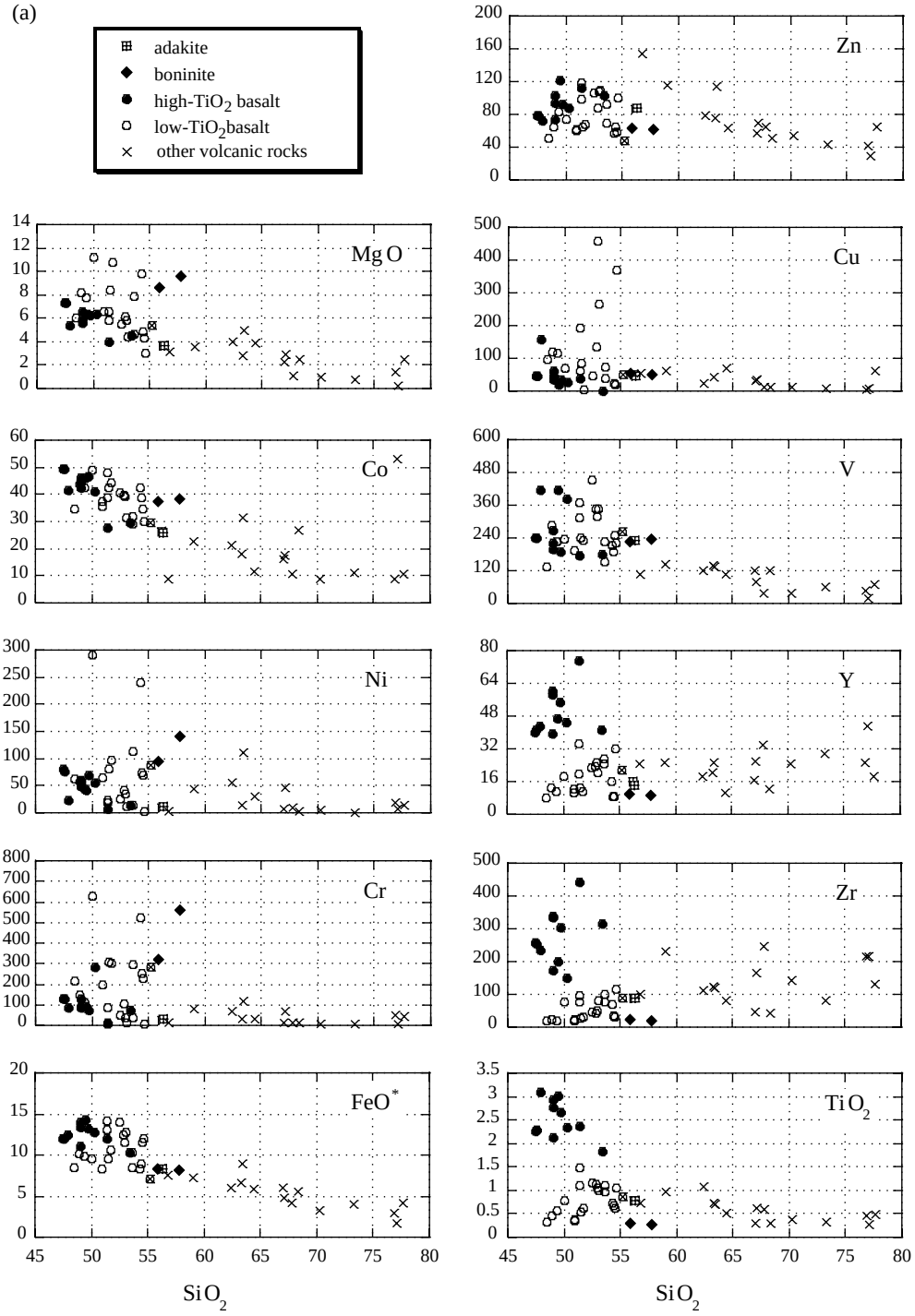

Fig. 3. Silica variation diagrams of the Devonian volcanic rocks from the Altay area, Xinjiang, China. Some basalts and andesites have high MgO (ca. 10 wt%), Ni (200–300 ppm) and Cr (500–650 ppm) suggesting the presence of primitive magmas in the area. Large scatter of Rb, K_2O and Na_2O is probably due to alteration of the constituent minerals.

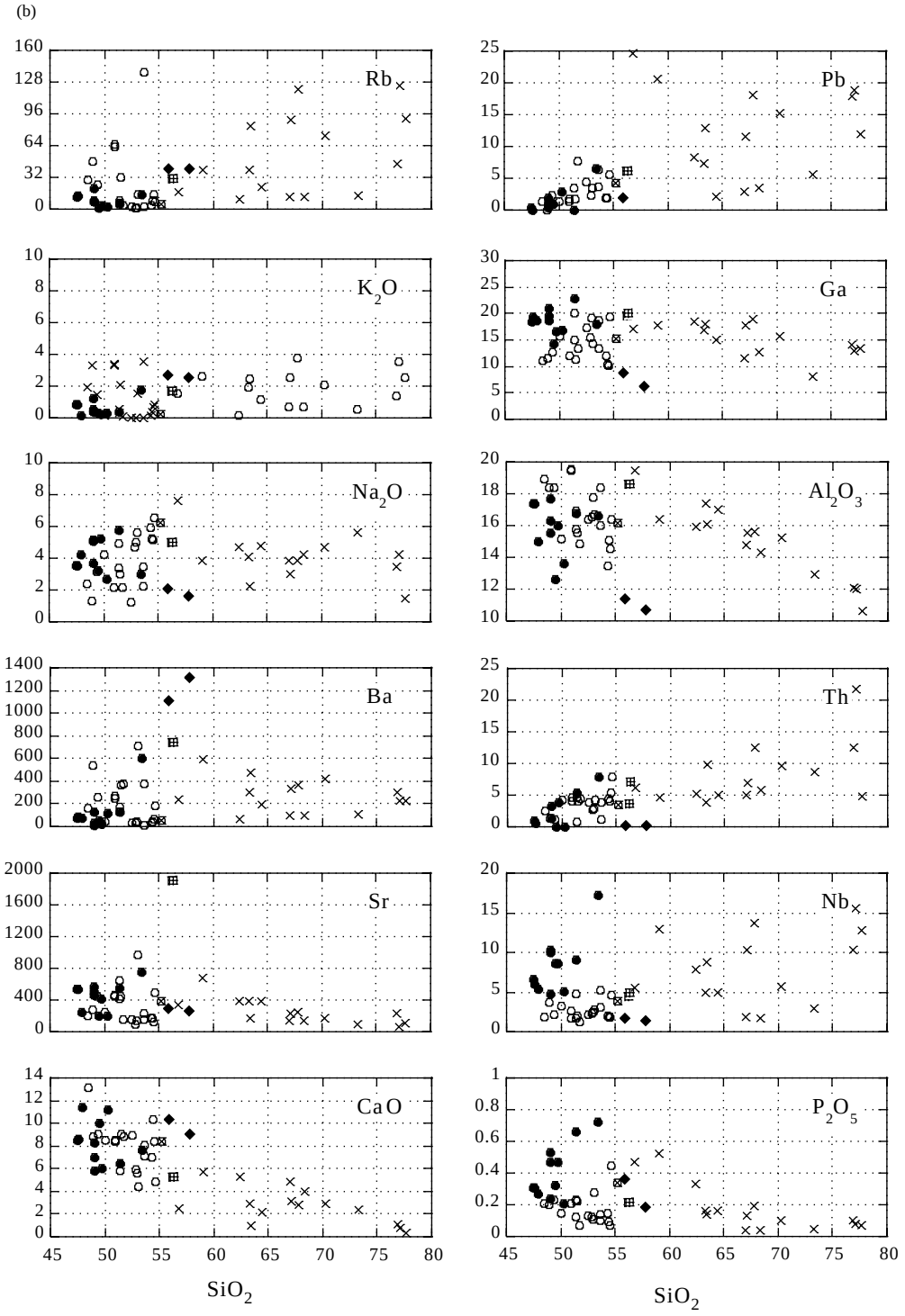

Fig. 3 (*continued*)

1980). Although boninite is presumed to be a hydrous partial melt of mantle peridotite, its melting temperature has been suggested to be high (1100–1200 °C), and may require a regional thermal anomaly for its generation (Crawford et al., 1989; Macpherson and Hall, 2001). In the southern Altay region, boninites occur in the Saerbulake area as pillow lava or pillow breccia. The rocks are metamorphosed, but retain the original porphyritic textures consisting ca. 15 vol% phenocrysts of clinopyroxene, olivine, and plagioclase. The relict clinopyroxene has Mg# (=100*Mg/(Mg+Fe)) of 90–92, with Cr_2O_3 contents of 0.5–0.7 wt%. The boninites are characterized by low and U-shaped REE patterns, low HFS elements and also high Ba (1100–1300 ppm) content. Sr and Nd isotopic compositions (Table 4) are moderately depleted, common to

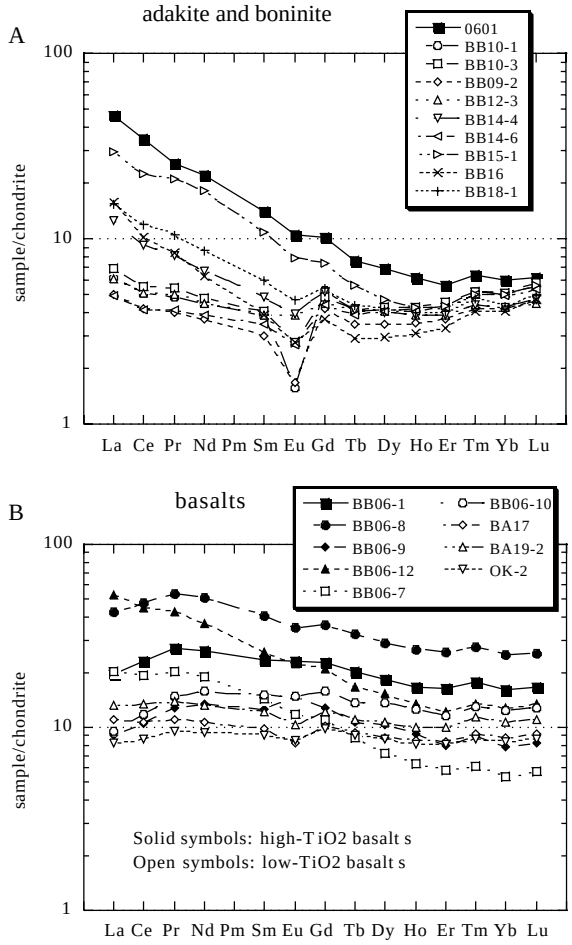

Fig. 4. Chondrite-normalized REE pattern of Devonian volcanic rocks of Altay area, Xinjiang, China; (A) adakite and boninite, (B) basalt and gabbros. Normalizing values after Nakamura et al. (1974). Adakites show depletion in HREEs. Boninites show ranges of La/Lu ratios. Low La/Lu boninites show slightly U-shaped uniformly-depleted REE pattern with Eu negative anomaly, whereas, high La/Lu boninites without Eu negative anomaly.

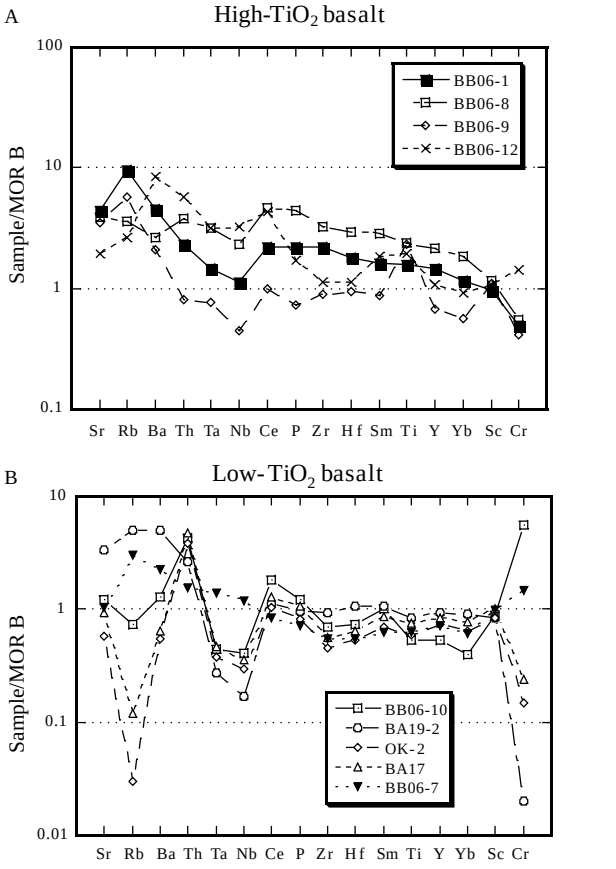

Fig. 5. Spider diagrams of representative Devonian basalts of Altay area, Xinjiang, China. Original data are normalized to average NMORBs after Sun and McDonough (1989), (A) represents high-TiO_2 basalts, and (B) represents low-TiO_2 basalts.

boninite of other localities (Cameron et al., 1983). The depleted nature of TiO_2 and other HFSE is consistent with the high Cr/(Cr + Al) ratio of the chromian spinel inclusion in the augite phenocryst. The Mg/(Mg + Fe) ratio and Cr content of the clinopyroxene phenocryst is similar to those of mantle clinopyroxene (e.g. Parkinson and Pearce, 1998), indicating that the phenocyrst crystallized from primitive magma. The chromian clinopyroxene phenocryst in the boninite is almost in Mg–Fe partition equilibrium with the bulk rock composition ($K_{Fe-Mg} = 0.20$, and if we assume Fe^{3+}/total Fe of 0.2). The bulk rock of the Altay boninites could therefore represent the primary magma composition derived from partial melting of hydrous upper mantle peridotite. In other words, the primary magma of the Altay boninite had an MgO content of 8–10 wt%, SiO_2 ranging from 56 to 58 wt%, CaO contents of 9–10 wt%, Al_2O_3 contents of ca. 11 wt%, and TiO_2 contents of 0.25 wt%.

Melting experiments on high-magnesian andesites have been carried out by many researchers (Tatsumi, 1982; Kushiro and Sato, 1978; Umino and Kushiro, 1989; van der Laan et al., 1989; Klingenberg and Kushiro, 1996; Hirose, 1997; Falloon and Danyushevsky, 2000). As noted previously, the Saerbulake boninite can be classified as a Ca-rich boninite (Crawford et al., 1989). The experiments by Falloon and Danyushevsky (2000) was aimed to resolve the conditions of generation of high-Ca boninite, but their estimated primitive high-Ca boninite was extremely high in MgO contents (19–24 wt%), and the estimated generation temperature (1480 °C) may not be applicable for the origin of the Altay high-Ca boninite. Among other experiments, Hirose (1997) showed that the SiO_2 content of melt in water-saturated melting experiments of lherzolite is well correlated with the temperature of melting. The SiO_2 content of 56–58 wt% may therefore be produced at temperatures of 1000–1050 °C and 1 GPa pressure. Such melts have CaO contents of 8–10 wt%, similar to the Altay boninites. Although available experimental work is insufficient to constrain explicitly the conditions of formation of the Altay boninite, we suggest that the Altay high-Ca boninite formed by melting of refractory mantle peridotite fluxed by a slab-derived fluid component at temperatures of 1000–1050 °C and 1 GPa pressure under water saturated conditions. These conditions correspond to mantle potential temperature of 1200–1300°C

(McKenzie and Bickle, 1988), and nearly coincides with those of MORBs at oceanic ridges. Therefore, the boninite formed at usual mantle potential temperatures.

5.2. Geochemical features of basaltic rocks

The basaltic rocks of the present work are classified into high-TiO_2 and low-TiO_2 basalts, which show variable trace element enrichment patterns. Many of the low-TiO_2 basalts of the Saerbulake and Ashele areas show depletion of Ta and Nb relative to Th and Ce (Fig. 5B), suggesting they represent island arc tholeiite in the Devonian Altay. One basalt from the Kekesentao area (No. BB06-7, #1302) shows a flat pattern in the spider diagram (Fig. 5A) and a slightly LREE enriched pattern (Fig. 4B), similar to that of transitional MORB; i.e. between depleted N-MORB and E-MORB. It is likely that the sample represents oceanic crust of the paleo-Asian Ocean in Devonian time.

High-TiO_2 basalts and gabbros occur in the Suoerkuduke, Saerbulake, and Kuerti areas. Xu et al. (2002) already pointed out that basalts of the Kuerti section have geochemical features of back-arc basin basalts; i.e. transitional between arc tholeiite and MORB. The high-TiO_2 basalts of Saerbulake have flat trace element patterns with mild depletions of Ta and Nb, transitional between arc tholeiite and MORB composition. They are characterized by high $\varepsilon_{Nd}(T)$ (4.8, 5.2). The presence of titanaugite in the groundmass suggests that they represent alkalic basalts. The high-TiO_2 basalts of the Suoerkuduke area show even higher enrichment of Nb compared with those of Saerbuduke, suggesting that the composition is more like oceanic island basalts. Fig. 5A also shows that a high-TiO_2 gabbro (BB06-8) has an intraplate basalt-like trace element pattern. The high abundance of REE in the gabbro is consistent with an OIB origin. Dobretsov et al. (2004) described an OIB-type basalt in Gorny Altay (northern Altay) associated with limestones and suggested the oceanic island contribution in the formation of continental crust in Altaids. Identification of an OIB-type gabbro in the southern Altay reinforces the contribution of oceanic islands in the formation of continental crust in the Devonian Altay. As a whole, the basaltic rocks in the southern Altay illustrate a range of geochemical features from arc tholeiite, through transitional back-arc basin basalt, to MORBs and OIBs.

5.3. Tectonic significance of the volcanic rocks of Altay

The most notable feature of the Devonian formations in the southern Altay is the juxtaposition of volcanic rocks of various origins even within a limited area; i.e. the adakite and the boninites are, respectively, associated with high-TiO_2 and low-TiO_2 basalts and/or gabbros. These rocks mostly occur as tectonic mélanges. Therefore, it is suggested that complex accretion and tectonic processes including thrusting, duplex formation, strike-slip faulting, and serpentine diapirs were active during convergence in the Devonian–Carboniferous paleo-Asian ocean between the Siberian and Junggar plates.

Adakite and boninite are of particular tectonic significance. Adakite generally occurs in the volcanic front where young slab is subducting (Defant and Drummond, 1990). Although adakite could be generated by lower crustal melting of thick continental crust (Martin, 1993), the Suoerkuduke adakite more likely represents low-degree partial melting of subducted young oceanic crust, somewhat affected by interaction with mantle wedge peridotite and sediment incorporation. Boninites generally occur in a fore-arc tectonic setting, as manifested in the Izu-Bonin and Tonga arcs (Crawford et al., 1989). There are several possible models of boninite generation, such as subduction of an active spreading center, initiation of subduction accompanied by asthenospheric upwelling, incipient splitting of an island arc by a MORB-source diapir, and fore-arc spreading (Kim and Jacobi, 2002). Ophiolites, representing sections of oceanic crust, are often associated with boninites (Gillis and Banerjee, 2000; Ishikawa et al., 2002). This may partly be inevitable, because obduction and uplifting of oceanic crust should be associated with initiation of subduction, which supply arc-type volcanic rocks to the section of oceanic crust. Another possible model for the close association of boninite in ophiolite is when slab breakoff during continent–continent collision causes upwelling of asthenospheric material, which in turn supplies heat to the forearc region in order to generate boninitic rocks. Davies and von Blanckenburg (1995) pointed out by numerical modeling that shallow slab breakoff may take place where buoyant continental plates collide with subducting oceanic slab. The Altaid orogenic belt is wide and formed through a long period accretion of microplates in Paleozoic time. We envisage that repeated rifting formed the paleo-Asian ocean with NMORB basaltic crust. The paleo-Asian ocean may have included intraplate volcanism that formed oceanic islands. The paleo-Asian ocean might have then narrowed by convergence at subduction zones, where abundant island arc tholeiitic and calc-alkalic igneous activity occurred. Adakite might have formed where young oceanic slab subducted. The subduction locally formed marginal basins, where transitional back-arc basin basalt occurred. The subduction may have been interupted when two continents or microcontinents collided, where slab breakoff took place with subsequent magmatism of boninite and related rocks due to local upwelling of asthenosphere. Although the closure of the paleo-Asian Ocean is suggested to have taken place in the Carboniferous (Li and Xiao, 1999; Yu et al., 1995), slab breakoff might have taken place when one of the microplates or buoyant continental fragments collided against either the Siberian or Junggar plates. Juxtaposition of adakite, boninite, and various types of basaltic rocks in the southern Altay Devonian rocks, is therefore the result of a sequence of formation, cessation and closure of the paleo-Asian ocean in Devonian time between the Junggar and Siberian lithospheres.

6. Conclusions

Adakite occurs in the Suoerkuduke area of the southern Altay as a clastic deposit mainly composed of fragments of hornblende andesite and pyroxene andesite. The rock has

high Sr/Y ratios (120–136), and intermediate Y content (14–16 ppm), indicating that they represent products of low degree melting of oceanic crust in a young subducting slab.

Boninite occurs in the Saerbulake area of the southern Altay. It contains relict high-Cr augite with Mg# of 90–92. The primary magma composition of the boninite may have had a MgO content of ca. 10 wt%, and the depleted characteristics in HFS elements suggest generation from depleted sub-arc mantle fluxed by slab-derived fluid. It is possible that the boninite may have been generated at the time of continent–continent collision, where previously subducting slab may have broken off. Local injection of sub-slab asthenosphere heated the depleted mantle peridotite in the fore-arc area accompanied by a flux of slab-derived fluids.

Basalts and gabbros show variable geochemical features from island-arc tholeiite, through transitional back-arc basin basalt, mid-oceanic ridge basalt and intraplate basalt.

Juxtaposition of such variable volcanic rocks in the southern Altay areas may have been caused by a sequence of rifting and convergence in the Devonian paleo-Asian Ocean between the Siberian and Junggar plates.

Acknowledgements

This work is the result of a China–Japan Cooperative Project for the study of high-magnesian volcanic rocks in China and Japan, funded by CNSF(40073006) and JSPS, and Major State Basic Research Program of the People's Republic of China (2001CB409805) for which we are much indebted. Constructive reviews by Prof. Jahn and Prof. Okamura were helpful in improving the content of the paper. Discussions with Prof. Keiichi Shiraki, Dr Jifeng Xu, Prof. Akira Ishiwatari, and Dr Keiko Suzuki-Kamata are much appreciated. English correction of the journal editorial office is much appreciated.

References

Arai, S., 1994. Characterization of spinel peridotites by olivine–spinel compositional relationships: review and interpretation. Chemical Geology 113, 191–204.

Cameron, W.E., McCulloch, M.T., Walker, D.A., 1983. Boninite petrogenesis: chemical and Nd–Sr isotopic constraints. Earth and Planetary Science Letters 65, 75–89.

Chen, B., Jahn, B.M., 2004. Genesis of post-collisional granitoids and basement nature of the Junggar Terrrane, NW China: Nd–Sr isotope and trace element evidence. Journal of Asian Earth Sciences 23, 691–703.

Crawford, A.J., Falloon, T.J., Green, D.H., 1989. Classification, petrogenesis and tectonic setting of boninites. In: Crawford, A.J. (Ed.), Bonitnites. Unwin Hyman, London, pp. 1–49.

Davies, J.H., von Blanckenburg, F., 1995. Slab breakoff: a model of lithosphere detachment and its test in the magmatism and deformation of collisional orogens. Earth and Planetary Science Letters 129, 85–102.

Defant, M.J., Drummond, M.S., 1990. Derivation of some modern arc magmas by melting of young subducted lithosphere. Nature 347, 662–665.

Dobretsov, N.L., Buslov, M.M., Uchio, Y., 2004. Fragments of oceanic islands in accretion–collision areas of Gorny Altai and Salair, southern Siberia, Russia: early stages of continental crustal growth of the Siberian continent in Vendian-Early Cambrian time. Journal of Asian Earth Sciences 23, 673–690.

Falloon, T.J., Danyushevsky, L.V., 2000. Melting of refractory mantle at 1.5, 2 and 2.5 GPa under anhydrous and H_2O-undersaturated conditions: implications for the petrogenesis of high-Ca boninites and the influence of subduction components on mantle melting. Journal of Petrology 41, 257–283.

Gillis, K.M., Banerjee, N.R., 2000. Hydrothermal alteration patterns in supra-subduction zone ophiolite. Geological Society of America, Special Paper 349, 283–297.

Hirose, K., 1997. Melting experiments on lherzolite KLB-1 under hydrous conditions and generation of high-magnesian andesitic melts. Geology 25, 42–44.

Hu, A.Q., Jahn, B.M., Zhang, G.X., Chen, Y.B., Zhang, Q.F., 2000. Crustal evolution and phanerozoic crustal growth in northern Xinjiang: Nd isotopic evidence. Part 1. Isotopic characterization of basement rocks. Tectonophysics 328, 15–51.

Ishikawa, T., Nagaishi, K., Umino, S., 2002. Boninitic volcanism in the Oman ophiolite: implications for thermal condition during transition from spreading ridge to arc. Geology 30, 899–902.

Ishiwatari, A., 1985. Igneous petrogenesis of the Yakuno ophiolite (Japan) in the context of the diversity of ophiolites. Contributions to Mineralogy and Petrology 89, 155–167.

Jahn, B.M., Wu, F.Y., Chen, B., 2000. Granitoids of the central Asian orogenic belt and continental growth in the phanerozoic. Transactions of the Royal Society of Edinburgh, Earth Sciences 91, 181–193.

Jahn, B.M., Windley, B., Natal'in, B., Dobretsov, N., 2004. Phanerozoic continental growth in central Asia. Journal of Asian Earth Sciences 23, 599–603.

Kim, J., Jacobi, R.D., 2002. Boninites: characteristics and tectonic constraints, northeastern Appalachians. Physics and Chemistry of the Earth 27, 109–147.

Klingenberg, B.M.E.T., Kushiro, I., 1996. Melting of a chromite-bearing harzburgite and generation of boninitic melts at low pressures under controlled oxygen fugacity. Lithos 37, 1–14.

Kushiro, I., Sato, H., 1978. Origin of some calc-alkalic andesites in the Japanese Islands. Bulletin Volcanologique 41, 576–585.

Li, X.H., 1997. Geochemistry of the Longsheng ophiolite from the southern margin of Yangtze craton, SE China. Geochemical Journal 31, 323–337.

Li, J.Y., Xiao, X.C., 1999. Brief reviews on some issues of framework and tectonic evolution of Xinjiang crust, NW China. Scientia Geologica Sinica 34, 405–419.

Liang, X.R., Wei, G.J., Li, X.H., Liu, Y., 2003. Precise measurement of $^{143}Nd/^{144}Nd$ and Sm/Na ratios using multiple-collectors inductively coupled plasma-mass spectrometer (MC-ICPMS). Geochimica 32, 91–96 (in Chinese with English abstract).

Macpherson, C.G., Hall, R., 2001. Tectonic setting of eocene boninite magmatism in the Izu-Bonin-Mariana forearc. Earth and Planetary Science Letters 186, 215–230.

Martin, H., 1993. The mechanisms of petrogenesis of the archean continental crust-comparison with modern processes. Lithos 30, 373–388.

McKenzie, D.P., Bickle, M.J., 1988. The volume and composition of melt generated by extension of the lithosphere. Journal of Petrology 29, 625–679.

Nagao, T., Kakubuchi, S., Shiraki, K., 1997. Quantitative major and trace element analyses of rocks by X-ray fluorescence spectrometry (Rigaku/RIX3000). Report of Center for Instrumental Analysis, Yamaguchi University, 5, 10–15.

Nakamura, N., Masuda, A., Shimizu, H., 1974. Determination of REE, Ba, Fe, Mg, Na and K in carbonaceous and ordinary chondrites. Geochimica et Cosmochimica Acta 38, 757–775.

Niu, H.C., Xu, J., Yu, X.Y., Chen, F.R., Zheng, Z.P., 1999. Discovery of Mg-rich volcanic rock series in western Altay area, Xinjiang and its geologic significance. Chinese Science Bulletin 44, 1685–1687.

Parkinson, I.J., Pearce, J.A., 1998. Peridotites from the Izu-Bonin-Mariana forearc (ODP Leg 125): evidence for mantle melting and melt-mantle interaction in a supra-subduction zone setting. Journal of Petrology 39, 1577–1618.

Rapp, P.R., Watson, E.B., 1995. Dehydration melting of metabasalt at 8–32 kbar: implications for continental growth and crust-mantle recycling. Journal of Petrology 36, 891–931.

Robinson, P.T., Zhou, M.F., Hu, X.F., Reynolds, P., Wenji, B., Yang, J., 1999. Geochemical constraints on the origin of the Hegenshan ophiolite, inner Mongolia, China. Journal of Asian Earth Sciences 17, 423–442.

Sen, C., Dunn, T., 1994. Dehydration melting of a basaltic composition amphibolite at 1.5 and 2.0 GPa: implications for the origin of adakites. Contributions to Mineralogy and Petrology 117, 394–409.

Şengör, A.M.C., Natal'in, B.A., Burtman, V.S., 1993. Evolution of the Altaid tectonic collage and palaeozoic crustal growth in Eurasia. Nature 364, 299–307.

Shiraki, K., Kuroda, N., Urano, H., Maruyama, S., 1980. Clinoenstatite in boninites from the Bonin Islands, Japan. Nature 285, 31–32.

Springer, W., Seck, H.A., 1997. Partial fusion of basic granulites at 5 to 15 kbar: implications for the origin of TTG magmas. Contributions to Mineralogy and Petrology 127, 30–45.

Sun, S.S., McDonough, W.F., 1989. Chemical and isotopic systematics of ocean basalts: implication for mantle composition and processes. In: Saunders, A.D., Norry, M.J. (Eds.), Magmatism in Ocean Basins. Geological Society of London Special Publication 42, pp. 313–345.

Tatsumi, Y., 1982. Origin of high-mangesian andesites in the Setouchi volcanic belt, southwest Japan. II. Melting phase relations at high pressures. Earth and Planetary Science Letters 60, 305–317.

Taylor, R.N., Nesbitt, R.W., Vidal, P., Harmon, R.S., Auvray, B., Croudace, I.W., 1994. Mineralogy, chemistry and genesis of the boninite series volcanics, Chichijima, Bonin Islands, Japan. Journal of Petrology 35, 577–617.

Umino, S., Kushiro, I., 1989. Experimental studies on boninite petrgenesis. In: Crawford, A.J. (Ed.), Boninites and Related Rocks. Allen & Unwin, New Zealand, pp. 89–111.

van der Laan, S.R., Flower, M.J., Koster van Groos, A.F., 1989. Experimental evidence for the origin of boninites; near-liquidus phase relations to 7.5 kbar. In: Crawford, A.J. (Ed.), Boninites and Related Rocks. Allen & Unwin, New Zealand, pp. 112–147.

Wang, G., Cheng, S., Yang, S., Zhang, Z.M., Ou, Y.S., 1995. Map of Tectonism-Formation in the Northern Xinjiang China and Its Neighboring Area, 1/1500000. Geological Institute of China University Press.

Wang, Z.H., Sun, S., Hou, Q.L., Li, J.L., 2001. Effect of melt-rock interaction on geochemistry in the Kudi ophiolite (western Kunlun Mountains, northwestern China): implication for ophiolite origin. Earth and Planetary Science Letters 191, 33–48.

Xiong, X.L., Zhao, Z.H., Bai, Z.H., Mei, H.J., Wang, Y.X., Wang, Q., Xu, J.F., Niu, H.C., Bao, Z.W., 2001. Adakite-type sodium-rich rocks in Awulale mountain of west Tianshan: significance for the vertical growth of continental crust. Chinese Science Bulletin 46, 811–817.

Xu, J.F., Wang, Q., Yu, Y.X., 2000. Geochemistry of high-Mg andesites and adakitic andesite from the Sanchazi block of the Mian-Lue ophiolitic mélange in the Qinlin Mountains, central China: evidence of partial melting of the subducted Paleo-Tethyan crust. Geochemical Journal 34, 359–377.

Xu, J.F.,Chen, F.R., Yu, X.Y., Niu, H.C., Zhenos, Z.P., 2001. Kuerti ophiolite in Altay area of north Xinjiang: Magmatism of an ancient back-arc basin. Acta petrologica et Mineratogica 20, 344–352.

Xu, J.F., Castillo, P.R., Chen, F.R., Niu, H.C., Yu, X.Y., Zhen, Z.P., 2003. Geochemistry of late Paleozoic mafic igneous rocks from the Kuerti area, Xinjiang, northwest China: implications for backarc mantle evolution. Chemical Geology 193, 137–154.

Yang, J.S., Robinson, P.T., Jiang, C.F., Xu, Z.Q., 1996. Ophiolites of the Kunlun mountains, China and their tectonic implications. Tectonophysics 258, 215–231.

Yu, X.Y, Mei, H.J., Jiang, F.Z., Luo, C.R., Liu, T.G., Bai, Z.H., Yang, X.C., Wang, J.D., 1995. Volcanic Rocks and Ore-Forming Processes of Altys Area, Northern Xinjiang, P.R. China. Science Press, Beijing. 244 pp.

Zhang, Q., Chen, Y., Zhou, D.J., Qian, Q., Jia, X., Han, S., 1998. Geochemical characteristics and genesis of Dachadaban ophiolite in North Qilian area. Sicence in China, Series D 41, 277–281.

Zhang, H.X., Niu, H.C., Terada, K., Yu, X.Y., Sato, H., Ito, J., 2003. Zircon SHRIMP U–Pb dating on plagiogranite from Kuerti ophiolite in Altay, north Xinjiang. Chinese Science Bulletin 48, 2231–2235.

Zhang, H.X., Niu, H.C., Yu, X.Y., Ito, J., Sato, H., Qiang, S., 2005. Late Paleozoic adakites and Nb-enriched basalts from northern Xinjiang, NW China: evidence for the southward subduction of the Paleo-Asian ocean. The Island Arc 14, 55–68.

Zhou, M.F., Robinson, P.T., Malpas, J., Aitchison, J., Sun, M., Bai, W.J., Hu, X.F., Yang, J.S., 2001. Melt/mantle interaction and melt evolution in the Sartohay high-Al chromite deposits of the Dalabute ophiolite (NW China). Journal of Asian Earth Science 19, 517–534.

Zonenshain, L.P., Savostin, L.A., 1981. Geodynamics of the Baikal rift zone and plate tectonics of Asia. Tectonophysics 76, 1–45.